



1 **Perfluorocyclobutane (PFC-318, $c\text{-C}_4\text{F}_8$) in the global**
2 **atmosphere**

3 Jens Mühle¹, Cathy M. Trudinger², Matthew Rigby³, Luke M. Western³, Martin K. Vollmer⁴,
4 Sunyoung Park⁵, Alistair J. Manning⁶, Daniel Say³, Anita Ganesan⁷, L. Paul Steele², Diane J.
5 Ivy⁸, Tim Arnold^{9,10}, Shanlan Li⁵, Andreas Stohl¹¹, Christina M. Harth¹, Peter K. Salameh¹,
6 Archie McCulloch³, Simon O'Doherty³, Mi-Kyung Park⁵, Chun Ok Jo⁵, Dickon Young³, Kieran
7 M. Stanley³, Paul B. Krummel², Blagoj Mitrevski², Ove Hermansen¹¹, Chris Lunder¹¹, Nikolaos
8 Evangeliou¹¹, Bo Yao¹², Jooil Kim¹, Benjamin Hmiel¹³, Christo Buizert¹⁴, Vasili V. Petrenko¹³,
9 Jgor Arduini^{15,16}, Michela Maione^{15,16}, David M. Etheridge², Eleni Michalopoulou³, Mike
10 Czerniak¹⁷, Jeffrey P. Severinghaus¹, Stefan Reimann⁴, Peter G. Simmonds³, Paul J. Fraser²,
11 Ronald G. Prinn⁸, and Ray F. Weiss¹

12

13 ¹Scripps Institution of Oceanography, University of California, San Diego, La Jolla, CA, USA

14 ²Climate Science Centre, CSIRO Oceans and Atmosphere, Aspendale, Victoria, Australia

15 ³School of Chemistry, University of Bristol, Bristol, UK

16 ⁴Laboratory for Air Pollution and Environmental Technology, Empa, Swiss Federal Laboratories for Materials
17 Science and Technology, Dübendorf, Switzerland

18 ⁵KNU, Kyungpook Institute of Oceanography, College of Natural Sciences, Kyungpook National University, South
19 Korea

20 ⁶Met Office Hadley Centre, Exeter, UK

21 ⁷School of Geographical Sciences, University of Bristol, Bristol, UK

22 ⁸Center for Global Change Science, Massachusetts Institute of Technology, Cambridge, MA, USA

23 ⁹National Physical Laboratory, Teddington, Middlesex, UK

24 ¹⁰School of GeoSciences, University of Edinburgh, Edinburgh, UK

25 ¹¹NILU, Norwegian Institute for Air Research, Kjeller, Norway

26 ¹²Meteorological Observation Centre (MOC), China Meteorological Administration (CMA), Beijing, China

27 ¹³Department of Earth & Environmental Sciences, University of Rochester, Rochester, NY, USA

28 ¹⁴College of Earth, Ocean, and Atmospheric Sciences, Oregon State University, Corvallis, OR, USA

29 ¹⁵Department of Pure and Applied Sciences, University of Urbino, Urbino, Italy

30 ¹⁶ISAC-CNR, Bologna, Italy

31 ¹⁷Edwards LTD, Burgess Hill, West Sussex, UK

32

33

34 *Correspondence to:* Jens Mühle (jmuhle@ucsd.edu)

35

36



37 **Abstract.** We reconstruct atmospheric abundances of the potent greenhouse gas *c*-C₄F₈ (perfluorocyclobutane,
38 perfluorocarbon PFC-318) from measurements of in situ, archived, firm, and aircraft air samples with precisions of
39 ~1–2 % reported on the SIO-14 gravimetric calibration scale. Combined with inverse methods, we found near zero
40 atmospheric abundances from the early 1900s to the early 1960s, after which they rose sharply, reaching 1.66 ppt
41 (parts per trillion dry-air mole fraction) in 2017. Global *c*-C₄F₈ emissions rose from near zero in the 1960s to ~1.2 Gg
42 yr⁻¹ in the late 1970s to late 1980s, then declined to ~0.8 Gg yr⁻¹ in the mid-1990s to early 2000s, followed by a rise
43 since the early 2000s to ~2.2 Gg yr⁻¹ in 2017. These emissions are significantly larger than inventory based emission
44 estimates. Estimated emissions from eastern Asia rose from 0.36 Gg yr⁻¹ in 2010 to 0.73 Gg yr⁻¹ in 2016 and 2017,
45 31 % of global emissions, mostly from eastern China. We estimate emissions of 0.14 Gg yr⁻¹ from Northern and
46 Central India in 2016 and find evidence for significant emissions from Russia. In contrast, recent emissions from
47 North Western Europe and Australia are estimated to be small (≤ 1 % each). We conclude that emissions from China,
48 India and Russia are likely related to production of polytetrafluoroethylene (PTFE, “Teflon”) and other
49 fluoropolymers that are based on the pyrolysis of hydrochlorofluorocarbon HCFC-22 (CHClF₂) in which *c*-C₄F₈ is a
50 known by-product. The semiconductor sector, where *c*-C₄F₈ is used, is estimated to be a small source. Without an
51 obvious correlation with population density, incineration of waste containing fluoropolymers is probably a minor
52 source, and we find no evidence of emissions from electrolytic production of aluminum in Australia. While many
53 possible emissive uses of *c*-C₄F₈ are known, the start of significant emissions may well be related to the advent of
54 commercial PTFE production in 1947. Process controls or abatement to reduce *c*-C₄F₈ by-product were probably not
55 in place in the early decades, explaining the increase in emissions. With the advent of by-product reporting
56 requirements to the United Nations Framework Convention on Climate Change (UNFCCC) in the 1990s, concern
57 about climate change and product stewardship, abatement, and perhaps the collection of *c*-C₄F₈ by-product for use in
58 the semiconductor industry where it can be easily abated, it is conceivable that emissions in developed countries
59 were stabilized and then reduced, explaining the observed emission reduction in the 1980s and 1990s. Concurrently,
60 production of PTFE in China began to increase rapidly. Without emission reduction requirements, it is plausible that
61 global emissions today are dominated by China and other developing countries, in agreement with our analysis. We
62 predict that *c*-C₄F₈ emissions will continue to rise and that *c*-C₄F₈ will become the second most important emitted
63 PFC in terms of CO₂-equivalent emissions within a year or two. The 2017 radiative forcing of *c*-C₄F₈ (0.52 mW m⁻²)
64 is small but emissions of *c*-C₄F₈ and other PFCs, due to their very long atmospheric lifetimes, essentially
65 permanently alter Earth’s radiative budget and should be reduced. Significant emissions outside of the investigated
66 regions clearly show that observational capabilities and reporting requirements need to be improved to understand
67 global and country scale emissions of PFCs and other synthetic greenhouse gases and ozone depleting substances.

68



69 1 Introduction

70 The perfluorocarbon (PFC) perfluorocyclobutane (*c*-C₄F₈, PFC-318, octafluorocyclobutane, CAS 115-25-3) is a very
71 long-lived and potent greenhouse gas (GHG) regulated under the Paris Agreement of the United Nations Framework
72 Convention on Climate Change (UNFCCC). Ravishankara et al. (1993) concluded that the most important
73 atmospheric loss process of *c*-C₄F₈ is Lyman- α photolysis resulting in an atmospheric lifetime of 3200 years. Later,
74 Morris et al. (1995) argued that if reactions of *c*-C₄F₈ with electrons and positive ions in the mesosphere and aloft are
75 irreversible, the lifetime could be reduced to 1400 years, which, on human timescales, is still essentially infinite. *c*-
76 C₄F₈ has a radiative efficiency of 0.32 W m⁻¹ ppb⁻¹ (parts per billion) and, assuming a 3,200 year lifetime, a global
77 warming potential of 9,540 on a 100-year timescale (GWP₁₀₀) (Myhre and Shindell et al., 2013; Engel and Rigby et
78 al., 2018). Due to the long lifetime and high radiative efficiency, emissions of *c*-C₄F₈ (and other perfluorinated
79 compounds) essentially permanently alter the radiative budget of Earth (Victor and MacDonald, 1999).
80 Lovelock (1971) predicted the accumulation of *c*-C₄F₈ in the global atmosphere, but to the best of our knowledge, the
81 earliest atmospheric measurements of *c*-C₄F₈ were presented in Sturges et al. (1995) and in the Ph.D. theses of
82 Travnicek (1998) and Oram (1999, discussed further below). Sturges et al. (2000) determined from one vertical
83 balloon-borne profile in 1994 that *c*-C₄F₈ mole fractions declined from ~1.1 ppt (parts per trillion) in the lower
84 atmosphere of the Northern Hemisphere (NH) to ~0.6 ppt in the stratosphere, while Harnisch (1999) reported that
85 Sturges et al. (1995) had found 0.4 ppt in the troposphere decreasing to ~0.1 ppt at 25 km in 1994, suggesting a
86 revised calibration scale. Harnisch et al. (1998; 1999) estimated from this atmospheric gradient global emissions of
87 1–2 Gg yr⁻¹ (kt yr⁻¹). Travnicek (1998) reported ~0.2 ppt in 1977 and ~0.7 ppt in 1997 in the NH troposphere, from
88 which Harnisch (2000) estimated average global emissions of 0.7 Gg yr⁻¹. Despite differences in early measurements
89 and emissions estimates, perhaps due to different calibration scales and analytical methods, these studies were
90 consistent with the accumulation of *c*-C₄F₈ in the global atmosphere.
91 Harnisch (1999, 2000) stated that *c*-C₄F₈ had limited economic relevance, with some use for plasma etching in the
92 semiconductor industry, that *c*-C₄F₈ can be formed via dimerization of tetrafluoroethylene (TFE), and that thermal
93 decomposition or combustion of polytetrafluoroethylene (PTFE) and other fluoropolymers (Morisaki, 1978) (during
94 waste disposal) possibly led to the accumulation of atmospheric *c*-C₄F₈.
95 Today we have stronger evidence for *c*-C₄F₈ emissions from the semiconductor and microelectronics industry as it
96 has been increasingly used since the 1990s for dry etching, chemical vapor deposition chamber cleaning and as
97 deposition gas (Bosch process). Compared to other fluorinated gases used for these processes, more selective
98 etching, cost reduction in plasma cleaning, easier abatement and hence potentially lower contribution to global
99 warming have been cited as advantages of *c*-C₄F₈ (e.g., Sasaki et al., 1998; Christophorou and Olthoff, 2001; Raju et
100 al., 2003; Kokkoris et al., 2008; and references therein). However, due to efficient abatement with modern emission
101 controls (up to 90 %), today's *c*-C₄F₈ emissions from this industry could also be small (Zhihong et al., 2001).
102 Recently there is also further evidence that the thermal decomposition of PTFE and other fluoropolymers can lead to
103 the formation of *c*-C₄F₈, TFE and hexafluoropropylene (HFP) (van der Walt et al., 2008; Bezuidenhoudt et al., 2017);
104 the resultant *c*-C₄F₈ could therefore be emitted to the atmosphere.



105 One potentially major source of *c*-C₄F₈ that seems to have received too little attention, is the production of TFE and
106 HFP monomers, the building blocks for PTFE, fluorinated ethylene propylene (FEP, TFE/HFP copolymer) and other
107 fluoropolymers, which involves pyrolysis of hydrochlorofluorocarbon 22 (HCFC-22, CHClF₂) as *c*-C₄F₈, the dimer
108 of TFE, is a by-product/intermediate of this process (Chinoy and Sunavala, 1987; Broyer et al., 1988; Gangal and
109 Brothers, 2015). This reaction can be steered towards HFP or *c*-C₄F₈ by controlling the dimerization of TFE to *c*-
110 C₄F₈ and the co-pyrolysis of *c*-C₄F₈ with TFE to HFP (Jianming, 2006). *c*-C₄F₈ could therefore be emitted during
111 TFE/HFP/PTFE/FEP production if it is not abated or recovered, e.g. for use in the semiconductor industry or for
112 pyrolysis with TFE to HFP at a later stage, perhaps at a different facility.

113 Several other, perhaps minor, emissive uses of *c*-C₄F₈ are also known (see Lewis, 1989; Chung and Bai, 2000;
114 Harnisch, 2000; Christophorou and Olthoff, 2001; Kim et al., 2002; Liu et al., 2008; and reference therein), e.g., in
115 aerolyzed foods, as a food packaging gas, in retinal detachment surgery, for contrast-enhanced ultrasound imaging,
116 in radar systems, as a specialty refrigerant (e.g., in submarines where R405A (43 % *c*-C₄F₈) can replace pure HCFC-
117 22 and chlorofluorocarbon CFC-12), as an electrically insulating dielectric gas (e.g., in mixtures with sulfur
118 hexafluoride, SF₆), as a medium for polymerization reactions, in fire extinguishers, to estimate the size of natural gas
119 and oil reservoirs, for leak detection of nuclear waste containers (Schmidbauer, N., personal communication, 2011)
120 and as a geohydrological tracer (Kass, 1998). Production of *c*-C₄F₈ for these uses, via the pyrolysis of HCFC-22 or
121 perhaps from 1,2-dichlorotetrafluoroethane (CFC-114) (Siegemund et al., 2016), may cause emissions as well. While
122 the two major atmospheric PFCs, tetrafluoromethane (CF₄) and hexafluoroethane (C₂F₆), and the minor PFC octa-
123 fluoropropane (C₃F₈) are released during primary aluminum production (Holliday and Henry, 1959; Tabereaux,
124 1994; Fraser et al., 2013), no evidence for *c*-C₄F₈ emissions from primary aluminum production has been presented
125 so far. Cai et al. (2018) presented evidence for negligible emissions of *c*-C₄F₈ from the similar electrolytic production
126 of rare earth elements in China. There are no known natural sources of *c*-C₄F₈. In summary, there may be multiple *c*-
127 C₄F₈ emission sources, but the extent and time evolutions of these various potential emission sources are unclear.

128 Saito et al. (2010) reported the first continuous, approximately four year long, in situ measurement record of *c*-C₄F₈
129 at two stations in the NH, with mean baseline 2006–2009 mole fractions of ~1.22 ppt at Cape Oshiishi (43.1° N,
130 145.3° E) and ~1.33 ppt at Hateruma Island (24.1° N, 123.8° E) (NIES calibration scale). Saito et al. (2010)
131 determined increase rates of 0.01–0.02 ppt yr⁻¹ and global emissions of 0.6 ± 0.2 Gg yr⁻¹.

132 Oram et al. (2012) published the first multi-decade long atmospheric record of *c*-C₄F₈ in the Southern Hemisphere
133 (SH). They combined previous measurements of sub-samples of the Cape Grim Air Archive (CGAA) for the SH
134 with air dates prior to 1994 (from Oram, 1999, converted to a new, 19.6 % lower calibration scale with an estimated
135 uncertainty of ≤ 7 %) with newer measurements of CGAA sub-samples with air dates after 1994 and a change of
136 analytical method after 2006. They found an increase of *c*-C₄F₈ at Cape Grim from 0.35 ppt in 1978 to ~0.8 ppt in
137 1995 and 1.2 ppt in 2010, with a current increase rate of ~0.03 ppt yr⁻¹. They reported that global *c*-C₄F₈ emissions
138 increased from ~0.9 Gg yr⁻¹ in the early 1980s to ~1.7 Gg yr⁻¹ in 1986 before declining to a minimum of ~0.4 Gg yr⁻¹
139 in 1993, after which they increased to ~1.1 Gg yr⁻¹ in 2006 and 2007 and may have stabilized. Oram et al. (2012)
140 noted that the global emissions determined by Saito et al. (2010) were lower than their estimate and suggested that
141 the underlying atmospheric rise rate measured by Saito et al. may be too small.



142 In summary, calibration differences between previous studies are significant, no multi-decadal $c\text{-C}_4\text{F}_8$ record for the
143 NH has been published, and global emissions have not been reassessed since Oram et al. (2012). Therefore our
144 primary goals have been to develop an independent gravimetric $c\text{-C}_4\text{F}_8$ calibration scale and to characterize the
145 abundance of $c\text{-C}_4\text{F}_8$ with high precisions in both hemispheres in order to determine updated historic and recent
146 global emissions. We present measurements of $c\text{-C}_4\text{F}_8$ with precisions of ~1–2 % on the SIO-14 calibration scale (~2
147 % accuracy) developed by the Scripps Institution of Oceanography (SIO) using instrumentation and calibration
148 methods of the Advanced Global Atmospheric Gases Experiment (AGAGE) program (Prinn et al., 2018). We
149 discuss historic atmospheric mole fractions of $c\text{-C}_4\text{F}_8$ based on measurements of the CGAA for the extra-tropical SH,
150 archived air samples from various sources for the extra-tropical NH, continuous atmospheric measurements in both
151 hemispheres at multiple remote AGAGE stations since mid-2010, combined with measurements of air extracted from
152 firn from both hemispheres. Using our measurements and inverse modelling methods, we infer global $c\text{-C}_4\text{F}_8$
153 emissions since the beginning of the 20th century until 2017. To improve our understanding of prominent $c\text{-C}_4\text{F}_8$
154 sources and source regions, we investigate regional $c\text{-C}_4\text{F}_8$ emission strengths as observed by the global AGAGE
155 network in eastern Asia, Europe, parts of Australia and Russia and by an aircraft campaign over India. We also
156 summarize and discuss available inventory based “bottom-up” emissions and compare them to the emissions we
157 determined with our atmospheric measurement based “top-down” approach.

158 2 Experimental methods

159 2.1 Instrumentation, data availability, and calibration

160 $c\text{-C}_4\text{F}_8$ and ~40 other halogenated compounds were measured by AGAGE in 2 L air samples with the “Medusa”
161 cryogenic pre-concentration system with gas chromatograph (GC, Agilent 6890) and quadrupole mass selective
162 detector (MSD) (Miller et al., 2008; Prinn et al., 2018). Data from twelve in situ measurements sites and fourteen
163 Medusa instruments were used. At Monte Cimone, Italy, $c\text{-C}_4\text{F}_8$ was measured with a commercial Adsorption-
164 Desorption System with gas chromatograph and mass spectrometer (ADS-GC/MS) (Maione et al., 2013). Table 1
165 shows the availability of in situ, archived air (Sect. 2.2), firn air (Sect. 2.3) and aircraft air sample (Sect. 2.4)
166 measurements with information for each site. For all measurements, each sample was alternated with a reference gas
167 (Prinn et al., 2000; Miller et al., 2008), resulting in up to 12 fully calibrated samples per day (Medusa and ADS-
168 GC/MS). The reference gases at each site were calibrated relative to parent standards at SIO.
169 $c\text{-C}_4\text{F}_8$ measurements are reported on the SIO-14 calibration scale as ppt dry-air mole fractions. The calibration scale
170 is based on four gravimetric halocarbon/nitrous oxide (N_2O) mixtures via a stepwise dilution technique with large
171 dilution factors for each step (10^3 to 10^5) (Prinn et al., 2000; 2001). High purity $c\text{-C}_4\text{F}_8$ (99.999 %, Matheson Trigas)
172 and N_2O (99.9997 %, Scott Specialty Gases) were further purified by repeated cycles of freezing (-196°C), vacuum
173 removal of non-condensable gases, and thawing. Artificial air (Ultra Zero Grade, Airgas) was further purified via an
174 absorbent trap filled with glass beads, Molecular Sieve (MS) 13X, charcoal, MS 5Å, and Carboxen 1000 at -80°C
175 (ethanol/dry ice). Zero air was measured to verify insignificant $c\text{-C}_4\text{F}_8$ and other halocarbon blank levels before
176 being spiked with the $c\text{-C}_4\text{F}_8/\text{N}_2\text{O}$ mixtures. The resulting mixtures of $c\text{-C}_4\text{F}_8$ in artificial air have prepared values of



177 ~1.3 ppt and the relative standard deviation of the calibration scale is 0.23 %. We estimate the uncertainties of the
178 calibration scale propagation from SIO to the sites to be ~0.6 % and the calibration scale uncertainty to be ~2 %.

179 The primary calibration instrument for the AGAGE network at SIO (La Jolla, California), Medusa 1, and all field
180 instruments used a Porabond Q (25 m, 0.32 mm I.D., 5 μ m film thickness, Varian) chromatographic main column
181 and, initially Agilent 5973, later 5975 series MSDs. The original Medusa design is described by Miller et al. (2008);
182 subsequently all Medusas were converted or newly built to measure nitrogen trifluoride (NF₃) (Arnold et al., 2012),
183 but this did not affect the *c*-C₄F₈ measurements methodology or the results. While 5975 MSDs are beneficial for
184 samples and compounds with very low mole fractions, precisions for *c*-C₄F₈ measurements of archived air samples
185 (3–7 replicates, see next section) were similar, i.e. better than ~0.01 ppt. Daily reference gas measurement precisions
186 slightly improved from ~0.02 ppt (~1.5–2 %) to ~0.01 ppt (~1–1.5 %) with the 5975 MSDs. Detection limits (3 times
187 baseline noise) for 2 L air samples were ~0.01–0.03 ppt, perhaps slightly better for 5975 MSDs.

188 In addition to calibrations, Medusa 1 was also used to measure in situ local ambient air and several archived air
189 samples (see Sect. 2.2). However, analysis of most archived air samples at SIO occurred on a second instrument,
190 Medusa 7, as it was equipped with a more sensitive 5975 MSD at that time. For these measurements, we temporarily
191 converted Medusa 7 to use a GasPro GSC (60 m, 0.32 mm I.D., Agilent) main column as it promised better
192 separation performance for several higher PFCs (Ivy et al., 2012) measured along with *c*-C₄F₈. Similarly, Medusa 9,
193 the instrument used to measure most CGAA samples at the Commonwealth Scientific and Industrial Research
194 Organisation (CSIRO, Aspendale) and ambient air after October 2010, had been converted to use a GasPro column.

195 On both types of main columns, *c*-C₄F₈ was measured on mass over charge ratios (*m/z*) of 131 (C₃F₅⁺) and 100
196 (C₂F₄⁺) and reported by height using carefully chosen integration parameters as perfluorobutane (C₄F₁₀) shares both
197 *m/z* and elutes on the tail of *c*-C₄F₈. The *m/z* ratios remained the same despite the very different separation principles
198 of these two main columns. Measurements of archived air samples on Medusa 7 with both main columns agreed
199 within less than 0.01 ppt (ratio of 1.0016, R² = 1.0000, n = 4, 0.237–1.11 ppt). In situ *c*-C₄F₈ measurements at SIO
200 with Medusa 1 (Porabond Q) and 7 (with the GasPro column) continued to agree within typical precisions. We also
201 compared archived air measurements on Medusa 1 and 7, both before and while Medusa 7 used the GasPro column,
202 and results agree within precisions of 0.02 ppt or better (Medusa 1 vs. Medusa 7, both Porabond Q, ratio of 1.0001,
203 R² = 0.9987, n = 95, 0.237–1.616 ppt, Medusa 1, Porabond Q vs. Medusa 7, GasPro, ratio of 1.0018, R² = 0.9979, n
204 = 39, 0.239–1.515 ppt). These tests show that the different main columns did not cause any bias.

205 The analytical systems showed no significant *c*-C₄F₈ blanks. The linearity of Medusa 7 (SIO) and 9 (CSIRO) used to
206 measure archived air samples was assessed with a series of diluted air samples (parent tank at 1.252 ppt, dilutions
207 from 100 % to 6.25 %, Ivy et al., 2012) and a series of different volumes of a working standard (parent tank at 1.60
208 ppt, sample volumes from 200 % to 5 % of usual 2 L volume). A small deviation from linearity was observed for the
209 most diluted samples and the smallest volumes probably due to a memory or blank of ~0.014 ppt on Medusa 9 was
210 corrected for. Medusa 7 showed perhaps an effect of ~0.008 ppt, but as this was just below the detection limits and
211 within the typical precisions, we chose not to correct for this.



212 2.2 Archived air samples of the extra-tropical Southern Hemisphere (SH, Cape Grim Air Archive, CGAA) 213 and extra-tropical Northern Hemisphere (NH)

214 To reconstruct the atmospheric history of $c\text{-C}_4\text{F}_8$ in the extra-tropical SH, 41 unique CGAA samples (collected
215 1978–2009, Langenfelds et al., 2014) were measured at CSIRO in 2011 (Ivy et al., 2012). Three CGAA tanks were
216 measured at the beginning, in the middle, and towards the end of the measurements at CSIRO, with agreements
217 within typical precisions or better (0.01–0.02 ppt). In addition, 8 SH samples were measured at SIO which were sub-
218 sampled from CGAA parent tanks (fill dates 1986–2008, 0.60–1.17 ppt) into evacuated stainless steel (SS) tanks (4.5
219 L, Essex Industries, USA) with a vacuum manifold and pressure regulator shown not to produce any $c\text{-C}_4\text{F}_8$ artefacts.
220 They were measured at SIO on Medusa 7 to take advantage of the more sensitive MSD and to evaluate the
221 agreement with Medusa 9 measurements at CSIRO. Four of these CGAA subsamples measured at SIO agreed within
222 precisions (delta mole fractions, $\Delta x = 0.00\text{--}0.01$ ppt, ratio = 1.0047, $R^2 = 0.9994$) with their CGAA parents measured
223 at CSIRO, 2 subsamples showed a larger differences (0.018 and 0.027 ppt). The measurements of the seventh
224 subsample and its CGAA parent were rejected, perhaps due to problems during the subsampling or with the parent
225 tank. While we did not measure the CGAA parent of the eights subsample at CSIRO, we found agreement ($\Delta x = 0.01$
226 ppt) with another CGAA tank of similar air age ($\Delta t = 63$ days) measured at CSIRO. Four additional SH samples (fill
227 dates 1995–2010, 0.84–1.25 ppt) were measured at SIO. Three were also in very good agreement with CGAA
228 samples of similar fill date measured at CSIRO ($\Delta x < 0.006$ ppt, $\Delta t = 7\text{--}23$ days) and one showed a larger difference
229 ($\Delta x = 0.05$ ppt). Based on an iterative filtering process designed to reject outliers greater than 2σ deviations from
230 curve fits through the results for all 60 SH samples (41 at CSIRO and 19 at SIO) and pollution filtered monthly mean
231 measurements (O'Doherty et al., 2001; Cunnold et al., 2002) at the extra-tropical stations CGO and ASA (Australia),
232 13 SH samples were rejected as outliers, leaving 47 SH samples (78 %).

233 To reconstruct the atmospheric history in the extra-tropical NH, 126 unique air samples mostly filled at SIO and
234 THD (1973–2016) were measured at SIO. Additionally, 3 NH samples (filled in 1980 and 1999) were measured at
235 CSIRO. Two of these tanks measured at CSIRO were filled together at SIO in 1999 with 2 tanks measured at SIO
236 and the agreement is excellent ($\Delta x = <0.007$ ppt). The third tank, filled in 1980 at Cape Meares, Oregon, agreed
237 within 0.034 ppt with another NH tank (filled at SIO within 9 days) measured at SIO. Despite this larger difference,
238 the overall good agreement of NH and SH samples measured at SIO and CSIRO shows that measurements on the
239 involved instruments were comparable and that calibration scales were properly propagated. Most of the NH samples
240 had been filled during baseline conditions for various purposes using modified diving compressors (RIX, SA-3 and
241 SA-6, Weiss and Keeling laboratories) and did not show any artefacts for many gases (e.g., Mühle et al., 2010;
242 O'Doherty et al., 2014; Vollmer et al., 2016). For $c\text{-C}_4\text{F}_8$, however, comparisons with concurrent in situ
243 measurements at MHD, THD, SIO and JFJ revealed artefacts for most of these samples and the iterative filtering
244 process only retained $c\text{-C}_4\text{F}_8$ data for eleven NH samples. In contrast, CGAA tanks had been filled with a cryogenic
245 method which did not produce any bias. Due to the sparse NH data and poor data quality before in situ measurements
246 started in the NH, the fits used for the iterative filtering process of NH data had to be guided by the final SH fit
247 shifted by 1.5 years to allow for the delay of $c\text{-C}_4\text{F}_8$ accumulation between the SH and NH due to inter-hemispheric
248 transport (Mühle et al., 2010; Vollmer et al., 2016). Without this guidance, initial NH fits were dominated by high
249 outliers, resulting in bad fits. Fig. 1 shows the filtered data and the final suggested fits.



250 2.3 Air extracted from firn

251 To augment the data set of in situ and archived air measurements, we measured *c*-C₄F₈ in samples from a subset of
252 the firn sites described in Trudinger et al. (2016), namely NEEM08 in the NH and DSSW20K and SPO01 in the SH,
253 plus one new site in the NH, Summit13, Greenland. We used the CSIRO firn model (Trudinger et al., 1997;
254 Trudinger et al., 2013) to characterize the age of the air in these samples (detailed in Sect. 4.1). Here, we give a brief
255 description of the firn sites. For a full description of the calibration of the CSIRO firn model for NEEM08,
256 DSSW20K, and SPO01 see Trudinger et al. (2013), for Summit13 see Fig. S1.

257 NEEM08: Firn air was extracted from the EU borehole in July 2008 in northern Greenland, drilled near the North
258 Greenland Eemian Ice Drilling Project (NEEM) deep ice core drilling site (77.45° N, 51.06° W) (Buizert et al.,
259 2012). This site has a moderate snow accumulation rate of 199 kg m⁻² yr⁻¹.

260 Summit13: Firn air was collected in May 2013 at Summit, Greenland from a borehole (72.66° N, 38.58° W) drilled
261 10 km NNW of Summit Station, Greenland. The US Firn Air system (Battle et al., 1996) was used to extract the air
262 from 19 depth levels in the firn from surface to just above bubble close-off (80.06 m). The 3 in borehole was drilled
263 with the Eclipse Ice Drill (IDDO) and new rubber bladders (1/8 in thick) were fabricated (Greene Rubber Co.,
264 Woburn, MA) for use in this campaign. 2.5 L glass flasks were filled at all depths for high resolution measurements
265 of gases performed by the National Oceanic and Atmospheric Administration (NOAA) (CO₂, CH₄, CO, N₂O, SF₆,
266 H₂). Larger volume samples from pre-selected depth levels were filled in 35 L electropolished SS tanks using a KNF
267 Neuberger pump (neoprene diaphragms). These samples were measured at SIO for *c*-C₄F₈ and a other trace gases
268 (including CH₄, N₂O, CFCs, HFCs, HCFCs, and SF₆). For quality control purposes, the sample line was measured on
269 site for [CO₂] and [CH₄] by CRDS (Los Gatos Research, μ-GGA) and [CO] by a Reducing Gas Detector (Peak Labs,
270 RCP1) prior to filling the flasks. Summit has a moderate snow accumulation rate of 211 kg m⁻² yr⁻¹. CSIRO firn
271 model calculations for Summit use the density profile from Adolph and Albert (2014) and mean annual temperature
272 and pressure of 241.75 K and 665 mbar. The diffusivity profile and related parameters were calibrated using the
273 measurements described above of CO₂, CH₄, N₂O, SF₆, CFC-11, CFC-12, CFC-113, CH₃CCl₃, HFC-134a, HCFC-
274 141b, and HCFC-142b. Firn model results for these tracers are shown in Fig. S1.

275 DSSW20K: Firn air was collected in January 1998 in Eastern Antarctica (66.73° S, 112.83° E) from a borehole
276 drilled 20 km west of the deep Dome Summit South (DSS) drill site near the summit of Law Dome (Smith et al.,
277 2000; Sturrock et al., 2002; Trudinger et al., 2002). This site has a short firn column and a moderate snow
278 accumulation rate of 150 kg m⁻² yr⁻¹.

279 SPO01: We only measured one sample collected in 2001 from 120 m from a borehole at the South Pole, Antarctica
280 (90° S, 119° W) (Aydin et al., 2004; Sowers et al., 2005). This site has a deep firn column and a low snow
281 accumulation rate of 75 kg m⁻² yr⁻¹, resulting in old firn air.

282 Firn air extracted from the DSSW20K, NEEM08, and SPO01 sites was measured at CSIRO in 2012 (Medusa 9),
283 while Summit13 firn air was measured at SIO (Medusa 7), see Table 1. *c*-C₄F₈ firn measurement data are included in
284 the data file listed in the Supplement. Other gases such as CH₄ and N₂O were measured as well.



285 2.4 Air samples collected over India and the Indian Ocean

286 Air samples were collected on-board the UK FAAM (Facility for Airborne Atmospheric Measurements) BAe-146
287 aircraft during eleven flights conducted from June 12, 2016 to July 9, 2016 (9–28° N, 72–86° E) into 3 L pre-
288 evacuated electropolished SS flasks (SilcoCan, Restek) sealed with metal bellow valves (SS-BNVVCR-4,
289 Swagelok). During the time it took to compress the air samples to 41 psig (30–60 s depending on altitude) using a
290 metal bellows pump (PWSC 28823-7, Senior Aerospace, USA), the aircraft travelled ~7 km. Nine flights occurred
291 over Northern India and two over Southern India and the Indian Ocean. In total, 176 flask samples were collected,
292 with the majority (>90 %) of these samples filled below 1.5 km altitude. The size of the subsamples analyzed with
293 the Medusa 21 at University of Bristol was reduced to 1.75 L (from 2 L) and the sampling rate to 50 ml min⁻¹ (from
294 100 ml min⁻¹) to allow for triplicate analyses of each flask and to accommodate for the lower flask pressure. *c*-C₄F₈
295 measurements are reported on the SIO-14 calibration scale. Detection limits, blanks, and precisions were similar to
296 those stated above. For further details, see Say et al. (2019).

297 3 Bottom-up emission inventories (UNFCCC, EDGAR, NIRs, WSC)

298 Emissions of compounds, such as *c*-C₄F₈, into the atmosphere are often estimated by so called “bottom-up” methods,
299 which are based on information such as purchased, produced or imported amounts, industrial activities referred to as
300 activity data and estimated emissions factors for each emissive process. Developed countries report annual emissions
301 of GHG, including *c*-C₄F₈, and ozone depleting substances (ODS) to the UNFCCC using such bottom-up methods.
302 These data are however, by definition, not representative of total global emissions as developing countries do not
303 have the same comprehensive UNFCCC reporting requirements, including countries such as South Korea, China,
304 and Taiwan with sizable electronics and PTFE manufacturing capacities and thus with potentially significant *c*-C₄F₈
305 emissions. An additional complication is that several countries report unspecified mixes of PFCs or of PFCs and
306 HFCs and other fluorinated compounds, making it difficult or impossible to estimate emissions of individual
307 compounds, such as *c*-C₄F₈. In the Supplement, we gather available inventory information from submissions to
308 UNFCCC, National Inventory Reports (NIRs), the Emissions Database for Global Atmospheric Research (EDGAR),
309 the World Semiconductor Council (WSC), and the US Environmental Protection Agency (EPA) in an effort to
310 estimate contributions from unspecified mixes and countries not reporting to UNFCCC to compile a meaningful
311 bottom-up inventory. Globally these add up to 10–30 t yr⁻¹ (0.01–0.03 Gg yr⁻¹, 1 t = 0.001 Gg) from 1990 to 1999,
312 30–40 t yr⁻¹ (0.03–0.04 Gg yr⁻¹) from 2000 to 2010, and 100–116 t yr⁻¹ (~0.1 Gg yr⁻¹) from 2011 to 2014 (with a
313 substantial fraction due to the U.S. emissions from fluorocarbon production reported by US EPA). Similar to what
314 had been pointed out by Saito et al. (2010) and Oram et al. (2012), we will show in Sect. 5.2 and 5.3 that
315 measurement based (“top-down”) global and most regional emissions are significantly larger than the compiled
316 bottom-up inventory information (see Fig. 5), similar to other PFCs (e.g., Mühle et al., 2010), reflecting the
317 shortcomings of current emission reporting requirements and emission inventories.



318 4 Modelling studies

319 4.1 CSIRO firn model

320 The CSIRO firn model and its use in global inversion frameworks has been described in detail (Trudinger et al.,
321 2013; Trudinger et al., 2016; Vollmer et al., 2016; Vollmer et al., 2018a; Vollmer et al., 2018b). Air samples taken
322 far away from pollution sources represent the background atmospheric trace gas composition at that time. Once air
323 enters the firn vertical diffusion and other physical processes in the firn lead to mixing of air of different ages.
324 Therefore, air extracted from firn must be described with an age distribution. We used the CSIRO firn model to
325 describe the relationship between trace gas mole fractions measured in each extracted air sample from a given depth
326 and the corresponding age distribution of high-latitude atmospheric mole fractions. The diffusion coefficient of c -
327 C_4F_8 relative to that of CO_2 in air at 253 K used here was 0.47 with an estimated uncertainty of ~10 %. This value
328 was determined using Equation 4 from Fuller et al. (1966) with Le Bas volume increments (e.g. Table 1.3.1, Mackay
329 et al. (2006) and a multiplier for the Le Bas increments of 0.97 (which minimizes the difference of calculated relative
330 diffusion coefficients of a number of compounds from values measured by Matsunaga et al. (1993, 2002, 2005)).
331 Figure 2 shows the measured depth profile of c - C_4F_8 (ppt) in air extracted from polar firn sites in the NH (Greenland)
332 and the SH (Antarctica), for site details see Table 1. All samples showed c - C_4F_8 mole fractions above the detection
333 limit. The firn reconstructed depth profiles are discussed in Sect. 4.3.1.

334 4.2 AGAGE 12-box model of the global atmosphere

335 The AGAGE 12-box two-dimensional model (Cunnold et al., 1983; Cunnold et al., 1997; Rigby et al., 2013)
336 describes the transport and loss of trace gases in the global atmosphere. The model divides the atmosphere into four
337 latitudinal bands at 0° and 30° S/° N and three altitude bands at 500 hPa and 200 hPa and calculates the mole
338 fractions in each box. The AGAGE background sites (MHD, THD, RPB, SMO and CGO, see Table 1) were
339 historically chosen to represent the trace gas mole fractions in the four lower (tropospheric) model “boxes”. Model
340 transport parameters were varied seasonally, but repeated annually. Given the very long atmospheric lifetime of c -
341 C_4F_8 compared to the study period, the lifetime of c - C_4F_8 was assumed to be infinite in the model.

342 4.3 Global inversion methods

343 We used the AGAGE 12-box model in two different Bayesian inversions, denoted as the “CSIRO” and “Bristol”
344 inversions, to estimate historic c - C_4F_8 emissions from our observations and to reconstruct historic abundances. Both
345 inversions used in situ and archive data and the CSIRO inversion additionally used firn data. The observations need
346 to be representative of clean background air at each sampling location. For in situ data, the AGAGE statistical
347 method was used to remove pollution events and to calculate pollution-free monthly mean background air mole
348 fractions for each AGAGE station (O’Doherty et al., 2001; Cunnold et al., 2002). As explained in Sect. 2.2, an
349 iterative filtering algorithm starting out with all the archived air data and the pollution-free monthly means was then
350 used to reject outliers for the extra-tropical SH and NH, mostly from the NH archive data. Due to the remoteness of
351 the firn sample sites, we assumed background conditions without any filtering.



352 4.3.1 CSIRO inversion

353 The CSIRO inversion was developed to infer annual emissions at the global scale from firn, ice core and atmospheric
354 measurements (Sturrock et al., 2002; Trudinger et al., 2002; Trudinger et al., 2016). Green's functions from the
355 CSIRO firn model were used to relate the measured air in the firn samples to air in the atmosphere in the past, and
356 Green's functions from the AGAGE 12-box model were used to relate global emissions with a specified latitudinal
357 distribution to mole fraction in the extra-tropical SH and NH. The inversion included constraints to avoid negative
358 mole fractions, negative emissions and unrealistic changes in emissions; these constraints were required due to the
359 characteristics of inverting firn data and sparse archive data. The uncertainty in reconstructed mole fractions and
360 inferred emissions was calculated using a bootstrap method that included the uncertainty in firn measurements,
361 annual mean mole fraction (this uncertainty is temporally-correlated, see Supplement in Vollmer et al., 2018a),
362 calibration scale ($\pm 2\%$), and the firn model through the use of an ensemble of Green's functions corresponding to
363 different firn model parameters (Trudinger et al., 2013; Trudinger et al., 2016; Vollmer et al., 2016).

364 Figure 3 shows the data that were used in the CSIRO inversion: annual values based on 10-year smoothing spline fits
365 (i.e. 50 % attenuation at periods of 10 years) to monthly means of pollution free in situ measurements at the AGAGE
366 background sites CGO (SH) and MHD (NH), annual values based on 10-year smoothing spline fits to measurements
367 of the CGAA and archived NH air samples, and air extracted from polar firn in both hemispheres. Annual means
368 from the spline were only used in the inversion when there were pollution free archive or in situ measurements
369 around that time. Figure 3 also shows the final reconstructed abundances for the extra-tropical SH (solid black line)
370 and NH (dashed black line) based on the optimized emissions. The measured mole fractions in firn air are plotted
371 against their effective atmospheric ages if that age is after 1965, where the effective ages are calculated using the
372 reconstructed history of atmospheric mole fractions determined by the CSIRO inversion (Trudinger et al., 2002).
373 Before 1965, the growth rate in the atmosphere was small and uncertain; this makes it difficult to determine effective
374 ages, so the earlier firn measurements are plotted against their mean ages. Firn depth profiles for each firn site
375 corresponding to the CSIRO inversion results are shown in Fig. 2 (solid lines) and they typically agree with the
376 measurements within precisions (1σ , shown as error bars).

377 Overall, the abundances reconstructed with the CSIRO inversion agree very well with the measurement data (also
378 see Fig. S2). In Fig. S3, we show the effect of excluding different sites from the inversion and the sensitivity of the
379 inversion to the relative diffusion coefficient of $c\text{-C}_4\text{F}_8$.

380 It should be pointed out that the deepest NEEM08 firn air sample for the NH showed slightly lower mole fractions
381 (0.0085 ppt) than the deepest DSSW20K samples for the SH (0.021 ppt and 0.0185 ppt), although the mean ages are
382 similar (1930s). The same applies to the second deepest NEEM08 (0.0105 ppt) and DSSW20K (0.018 ppt) samples
383 (1940s), which is unexpected for a long-lived anthropogenic compound predominantly emitted in the NH. While the
384 differences seem significant within the nominal precisions (0–0.0014 ppt) achieved for these firn samples measured
385 only 1–2 times, they are not significant within typical precisions achieved for archive samples ($\sim 0.01\text{--}0.02$ ppt)
386 which are typically measured 3 or more times and these data are just at or below the typical detection limits of 0.01–
387 0.03 ppt. Based on the order in which the firn samples were measured and the absence of detectable blanks, it seems
388 unlikely that a small blank, memory, calibration, or measurement problem could have caused this small discrepancy.
389 The early part of the reconstructed record, with near zero mole fractions, is also most susceptible to small



390 uncertainties in the calibrated diffusivity profiles versus depth for all sites used in the firm model, uncertainties in the
391 firm model structure (e.g., physical properties being invariant of time), or uncertainties in the diffusivity of different
392 tracers relative to each other. Thus, there are a number of possible reasons for the higher mixing ratio in the SH firm
393 data at this time, and we do not interpret this as evidence of higher mole fraction in the SH in the 1930s or 1950s.

394 **4.3.2 Bristol inversion**

395 The Bristol inversion was used to estimate annual fluxes of *c*-C₄F₈ using archive and in situ observations only (Rigby
396 et al., 2011; Rigby et al., 2014; Vollmer et al., 2018b). A priori, it was assumed that emissions were constant from
397 year to year, with an uncertainty in the year-to-year growth rate of 200 t yr⁻¹ (0.2 Gg yr⁻¹), approximately twice the
398 bottom-up estimate in Sect. 3. The derived emissions uncertainties include contributions from the measurement
399 repeatability, the calibration scale uncertainty, and the model-measurement representation error (Rigby et al., 2014).
400 Furthermore, because some archive air samples exhibit substantial short-timescale (< 1 year) variations that are
401 unlikely to represent real changes in the background atmosphere (Fig. 1), the minimum uncertainty was set to the
402 maximum deviation of the archive air samples from the smooth curve in Fig. 1 (0.03 ppt). Model representation
403 errors were estimated as the variability of the pollution-free monthly baseline means determined by the AGAGE
404 pollution algorithm (O'Doherty et al., 2001; Cunnold et al., 2002) from the high-frequency in situ data at each station
405 for each given month. For periods without in situ data, the representation error was assumed to be equal to the
406 average baseline variability from in situ data in the same latitudinal band scaled by the measured *c*-C₄F₈ abundance.
407 The calibration scale propagation uncertainty is estimated based on propagation uncertainties of the *c*-C₄F₈
408 calibration scale from primary gravimetric standards to secondary standards within the “R1” relative calibration
409 framework used in AGAGE and on propagation uncertainties from the R1 framework to the standards used to
410 measure individual samples. Figure 4 shows that there is good agreement between the archived air samples (Sect.
411 2.2) and the pollution free monthly mean in situ data from the AGAGE background sites (MHD and THD, RPB,
412 SMO, and CGO) used in the Bristol inversion and the reconstructed mole fractions for the four latitudinal bands
413 which these samples represent (see also Fig. S4).

414 **4.4 Regional model and inversion study using NAME-HB for eastern Asia**

415 To investigate regional emissions in eastern Asia (20° N–50° N and 110° E–160° E) from our observations we used
416 an inversion method based on Bayesian inference. We estimated annual mean emissions, assuming that emissions are
417 constant in both space and magnitude during each calendar year. Here, the inversion used observations from the
418 Gosan station as this site was operated with relatively few interruptions from October 2010 to the end of 2017, with
419 best data coverage from 2011 to 2015. These observations were binned into 12 hourly averages. The inversion
420 method requires an atmospheric transport model to derive the sensitivity of the observations to a surface emissions
421 field. We used the Lagrangian NAME (Numerical Atmospheric dispersion Modelling Environment) model from the
422 UK Met Office (Jones et al., 2007), driven by meteorology from the Met Office Unified Model (Walters et al., 2014).
423 The sensitivity was derived by releasing 20,000 hypothetical air parcels per hour of measurement from Gosan
424 station, which were transported backwards in time for up to 30 days. The model recorded the time and location that
425 air parcels interacted with the surface (below 40 m above ground level at a spatial resolution of 0.352° by 0.234°),



426 and these data were used to form an aggregated 30-day sensitivity or “footprint” map for each hour of measurement.
427 In addition, the model recorded the time and location that air parcels left the domain boundaries to provide the
428 sensitivity to the boundary conditions. The footprint maps, generated over the domain 5° S–74° N and 55° E–192° E
429 and up to 19 kilometres, were aggregated into 12 hourly averages.

430 We used a trans-dimensional hierarchical Bayesian method (NAME-HB) with a Metropolis-Hastings Markov chain
431 Monte Carlo (MCMC) algorithm (Metropolis et al., 1953; Hastings, 1970) to solve the inverse problem. This
432 allowed spatial emission estimates of *c*-C₄F₈ to be derived, whilst considering the uncertainties in the model,
433 measurements and a priori information and importantly the uncertainty in these uncertainties. Bayesian methods
434 require a priori knowledge, here the emissions and boundary conditions. As little information on eastern Asia’s *c*-
435 C₄F₈ emissions (see Sect. 3) was available, we based our mean a priori emissions on those estimated by Saito et al.
436 (2010). We spread their emissions for each reported country uniformly over the area of each country, rather than use
437 population density (as in Saito et al., 2010) as that is not likely to be a good proxy of *c*-C₄F₈ emissions. We also
438 spread 0.11 Gg yr⁻¹ of emissions over the rest of the domain where the footprint was calculated. The value of 0.11 Gg
439 yr⁻¹ is an approximate scaling of the global total emissions based on population in this outer domain, i.e. the
440 remainder of the domain not defined as eastern Asia. We do not report emission estimates outside of eastern Asia
441 due to large posterior uncertainties, but including them assisted with determination of the boundary conditions (or
442 non-proximal emissions). We assigned a large uncertainty to these a priori emissions (Table S1), which were
443 governed by a log-normal distribution, so that they were uninformative and the observations dominated the
444 estimation. We set a priori boundary conditions to be the mean background mole fractions measured at MHD on
445 each vertical boundary (N, E, W, S) of the NAME domain. Offsets to the boundary conditions on each boundary
446 were estimated in the inversion on a monthly basis.

447 The hierarchical nature of the inversion method means that hyper-parameters were also incorporated to include
448 uncertainties in the NAME sensitivities, which are described by a multivariate Normal distribution (see Ganesan et
449 al., 2014). The reversible jump, or trans-dimensional, aspect of the inversion means that the underlying resolution at
450 which the emissions are estimated is itself explored during inference (Lunt et al., 2016). Table S1 shows the a priori
451 probability distributions assigned to the emissions and boundary conditions scaling factors, model uncertainty and
452 underlying grid. The posterior emissions estimates and their uncertainties were governed by exploring the spaces of
453 each of these parameters and hyper-parameters.

454 **4.5 Regional model and inversion study using InTEM for Western Europe**

455 To investigate regional emissions in Western Europe (36° N–66° N and -14° E–31° E) we used InTEM, an inversion
456 framework (Arnold et al., 2018) based on the NAME Lagrangian transport model (Jones et al., 2007), together with
457 observations from MHD, Tacolneston (TAC), Jungfraujoch (JFJ) and Monte Cimone (CMN). A priori estimates
458 were considered unknown (see Sect. 3 and the Supplement) and therefore set to a uniform distribution of 0.2 Gg yr⁻¹
459 over the whole land area within the inversion domain with an uncertainty of 0–0.62 Gg yr⁻¹. Observational
460 uncertainty was time varying and estimated as the variability of the observations in a 6 hour moving window plus the
461 measurement repeatability determined from repeat measurements of the on-site calibration standards. Model
462 uncertainty was estimated every 2 hours as the larger of the median of all pollution events at each station in a year or



463 16.5 % of the magnitude of the pollution event. A temporal correlation of 12 hours was assumed in the model
464 uncertainty at each station. An analytical solution was found that minimized the residual between the model and the
465 observations and the difference between the posterior and the a priori flux estimate, balanced by the uncertainties of
466 both. The baseline was estimated in the inversion following Arnold et al. (2018). The variable resolution of the
467 inversion grid was calculated and refined within InTEM based on the magnitude of the footprint and emissions from
468 each grid box. The inversions were run 24 times per year, each time with a randomly generated sub-sample (90 %) of
469 the available observations from each station (10 % removed in 5-day blocks), to further explore the uncertainty.
470 Emissions and uncertainties were averaged across the 24 individual inversions thereby assuming 100 % correlation
471 between uncertainties in these separate inversions. 1-year inversions were performed covering the period 2013–2017.

472 **4.6 Regional model and inversion study using NAME-HB for India**

473 To investigate regional emissions from the Indian subcontinent from the samples taken on-board a research aircraft
474 in June and July 2016 (see Sect. 2.4) we used the NAME-HB inversion method described in Sect. 4.4 and Table S1.
475 Here, the domain spanned from 6° N to 48° N and from 55° E to 109° E with an altitude up to 19 kilometers and
476 emissions were estimated as the mean over the 2-month period. As with eastern Asia and Western Europe studies,
477 the sensitivity of the atmospheric measurements to surface emissions was derived using the NAME model. Back-
478 trajectories were simulated for each minute of each flight path for up to 30 days backward in time. To account for the
479 motion of the aircraft, hypothetical air parcels were released from a cuboid whose dimensions were defined as the
480 change in latitude, longitude and altitude of the aircraft during each 1 minute period, at a release rate of 1000 air
481 parcels min⁻¹. Wherever possible, samples were collected during periods of level flight, to minimise the altitude
482 component of the release volume. India's a priori emissions were set to 18 % of global *c*-C₄F₈ emissions (from Sect.
483 5.2), equal to India's fraction of the global population, but uniformly distributed over India. A large uncertainty was
484 assigned (Table S1) to reflect the lack of information on India's current *c*-C₄F₈ emissions. A priori vertical boundary
485 conditions were assigned using background mole fractions from MHD (N, E and W) and CGO (S). Offsets to these
486 boundary conditions were estimated in the inversion. We only report emissions for Northern and Central India (NCI)
487 as the inversion has low sensitivity over southern India and Sri Lanka and the north western edge of the domain and
488 no sensitivity beyond the Himalayas (see Fig. S5). Sensitivity tests indicate that *c*-C₄F₈ emissions determined for
489 NCI are insensitive to the choice of a priori emissions (see Fig. S6).

490 **4.7 Pollution events at Zeppelin station**

491 The Zeppelin (ZEP) station is located in a clean Arctic environment and receives air masses representative mostly of
492 the Arctic background. Nevertheless, 10 cases of enhanced *c*-C₄F₈ mole fractions were observed with the arrival of
493 air masses from Eurasia. To trace the origin of these events, we used 3-hourly 50-day backward simulations for a
494 passive tracer with version 10 of the Lagrangian particle dispersion model FLEXPART (Stohl et al., 2005). The
495 model was driven with operational meteorological analyses of the European Centre for Medium Range Weather
496 Forecasts (ECMWF, <https://www.ecmwf.int/>). The model set-up was similar to that typically used for inversion
497 studies (Stohl et al., 2009), but the number of events observed at the station was too small for a sensible regional
498 inversion. Instead, we inserted unit emission sources (~1 kg s⁻¹) at two facilities in Russia producing PTFE and



499 halogenated chemicals including *c*-C₄F₈ (HaloPolymer, Kirovo-Chepetsk, Kirov Oblast and Galogen Open Joint-
500 Stock Company, Perm), one or both of which we suspect to be responsible for most of the observed enhancements.
501 We then scaled the modeled *c*-C₄F₈ mole fractions based on these two unit sources to the observed enhancements to
502 estimate the source strength required to explain the observations. The two sources are quite close to each other and
503 thus very much correlated so it was impossible to quantify the influence of each source individually, but it turned out
504 that each source required about the same flux to produce a similar good match with the observations.

505 5 Results and discussion

506 5.1 Atmospheric histories of *c*-C₄F₈ in both hemispheres

507 Figure 1 shows the atmospheric histories of *c*-C₄F₈ in the extra-tropical NH and SH determined from several sets of
508 archive measurements and pollution filtered data from six in situ measurement stations. As detailed in Sect. 2.2, the
509 data shown have gone through an iterative filtering process which mostly removed outliers from the NH record. The
510 pollution free monthly mean in situ data for the four extra-tropical NH stations shown here and ZEP agree within
511 precisions, although JFJ data tends to be at the lower range since early 2015 for unknown reasons. The two extra-
512 tropical SH stations, CGO and ASA also agree well with each other. Mole fractions measured in both hemispheres
513 show a clear and consistent interhemispheric gradient reflecting the high precision of the measurements and
514 indicating that emissions of *c*-C₄F₈ predominantly occur in the NH. These data form a consistent atmospheric record
515 of *c*-C₄F₈ from the late 1970s to 2017 in both hemispheres, albeit with very sparse data for the NH before in situ
516 measurements started at JFJ and at other NH stations.

517 To augment our *c*-C₄F₈ data set and to extend our reconstruction further backwards in time, we measured air samples
518 extracted at several firm sites from both hemispheres and interpreted the data with the CSIRO global inversion
519 framework. The CSIRO inversion (see Sect. 4.3.1) yields the atmospheric history of *c*-C₄F₈ starting in 1900 until
520 present, although abundances are essentially not different from zero (<0.02 ppt) until the early 1960s (Fig. 3).
521 Average global *c*-C₄F₈ mole fractions reached 0.45 ppt in 1980, 0.74 ppt in 1990, 0.97 ppt in 2000, 1.29 ppt in 2010,
522 and 1.66 ppt in 2017. The Bristol inversion (see Sect. 4.3.2) does not incorporate firm data, still atmospheric histories
523 of the two inversions generally are in good agreement (see Fig. S7).

524 The CSIRO inversion reconstructs that the global rise rate of *c*-C₄F₈ accelerated from near zero before the late 1960s
525 to ~0.03–0.04 ppt yr⁻¹ in the mid-1970s to late 1980s, after which the rise slowed down to ~0.02 ppt yr⁻¹ in the early
526 1990s to mid-2000s. It increased again in the early 2000s and reached ~0.07 ppt yr⁻¹ in 2017.

527 Compared to Oram et al. (2012), our work extends the SH record from 2008 until present and, arguably, from 1978
528 back to 1900. Furthermore, it adds the full NH record. SH mole fractions reconstructed by Oram et al. (2012) are
529 very similar in 1978 and 1990, but ~0.06 ppt lower in the mid-1980s (~11 %) and the late 1990s to late 2000s (~5 %,
530 see Fig. S7). Although the stated precision in Oram et al. (2012) of 0.8 % (~0.01 ppt at 1.2 ppt) is similar to the 0.01–
531 0.02 ppt achieved here, the resulting precisions of the CGAA measurements achieved here are significantly
532 improved, e.g., the noise in the CGAA reconstruction by Oram et al. (2012) is about as large as the interhemispheric



533 gradient determined here (see Fig. S7). The estimated accuracy of the SIO-14 *c*-C₄F₈ calibration scale of ~2 % also
534 compares favorably to previous calibration scale uncertainties.

535 5.2 Global *c*-C₄F₈ emissions

536 Global *c*-C₄F₈ emissions (Fig. 5 and Supplement) started to increase in the early 1960s (CSIRO inversion) from near
537 zero to ~1.2 Gg yr⁻¹ in the late 1970s to the late 1980s. The Bristol inversion initially reconstructs lower emissions,
538 but catches up by the early 1980s, perhaps because firm data were not incorporated. After this, emissions determined
539 by both inversions declined to ~0.8 Gg yr⁻¹ in the mid-1990s to early 2000s. Since then emissions kept increasing,
540 reaching ~2.2 Gg yr⁻¹ in 2017. Both inversions reconstruct emissions which are significantly larger than available
541 bottom-up inventory information (see Sect. 3 and the Supplement), reflecting the shortcomings of the current
542 UNFCCC reporting requirements and inventories.

543 Emissions presented by Oram et al. (2012) agree very well from 2001 to 2007 with our results and on average also
544 from 1978 to 2001, although they show larger variability. Global emissions roughly estimated by Harnisch (2000)
545 based on measurements by Travnicek (1998) of ~0.7 Gg yr⁻¹ from 1978 to 1997 are lower than our estimate of $1.01 \pm$
546 0.10 Gg yr⁻¹. Saito et al. (2010) estimated global emissions of 0.6 ± 0.2 Gg yr⁻¹ from January 2006 to September
547 2009, about half of our 1.16 ± 0.09 Gg yr⁻¹ estimate. This is likely due to slowly changing *c*-C₄F₈ mole fractions in
548 calibration tanks used by NIES (Takuya Saito, personal communication, 2018), which would significantly affect the
549 background rise rate and thus global emissions, but would have had less influence on the regional emissions
550 estimated by Saito et al. (2010) as these are mostly dependent on the magnitude of the much larger pollution events
551 above background.

552 Global emissions of *c*-C₄F₈ have clearly not levelled off at 2005–2008 levels as had been suggested by Oram et al.
553 (2012), but kept rising. In contrast, emissions of other minor PFCs, C₂F₆ and C₃F₈, have decreased since the early
554 2000s and stabilized in recent years (Trudinger et al., 2016), reflecting that emission sources and/or use patterns of *c*-
555 C₄F₈ are different from those of the other minor PFCs. Weighted by GWP estimated 2017 emissions of *c*-C₄F₈, C₃F₈,
556 C₂F₆, and CF₄ were 0.021, 0.005, 0.022, and 0.083 billion tonnes of CO₂-eq., respectively (see Fig. S8). *c*-C₄F₈
557 emissions have been larger than those of C₃F₈ since 2004 and, assuming continued growth, will also outpace C₂F₆
558 emissions within a year or two, so that *c*-C₄F₈ will become the second most important PFC emitted into the global
559 atmosphere. In the next section, we will investigate regional emissions of *c*-C₄F₈ to gain a better understanding how
560 individual regions and sources may contribute to the global emissions.

561 5.3 Regional *c*-C₄F₈ emission studies

562 5.3.1 Emissions from eastern Asia

563 Within the AGAGE network, the two stations in eastern Asia, Gosan (GSN) and Shangdianzi (SDZ), show by far the
564 most frequent and most pronounced pollution events of up to ~14 ppt above NH background, indicating significant
565 regional emissions (see Fig. S9). Therefore, we use a regional inverse method (NAME-HB) to infer the emissions in
566 this region (20° N–50° N and 110° E–160° E, see Sect. 4.4). We focus on the observations from GSN as this site was
567 operated with relatively few interruptions from June 2010 to the end of 2017 and had almost full coverage for each



568 year from 2011 to 2015. Significantly longer data gaps exist for SDZ, which would have made interpretation of
569 inversion results more difficult. The sensitivity of the inversion generally decreases with distance to the receptor
570 station resulting in relatively low sensitivity for emissions from western China, eastern Japan and Taiwan (the
571 cumulative footprint map for 2010–2017 is shown in Fig. S10). Therefore, we report in Table 2 and Fig. 6 estimated
572 emissions for eastern China, western Japan, South Korea, North Korea, and Taiwan. *c*-C₄F₈ emissions in this eastern
573 Asian domain increased from 0.36 ± 0.07 Gg yr⁻¹ in 2010 to 0.73 ± 0.13 Gg yr⁻¹ in 2016 and 2017 and were
574 dominated by emissions from eastern China. Compared to the a priori emissions for eastern China of 0.185 Gg yr⁻¹,
575 which are based on the Saito et al. (2010) estimate for all of China for November 2007 to September 2009, this
576 represents an increase of ~62 % in 2010 and more than a tripling in 2017. Note, that if we were to sum up emissions
577 for all regions of China, including those where the inversion has low sensitivity, total emissions would be another
578 ~50–75 % higher. In contrast, the EDGAR 4.2 emission inventory, the only available bottom-up information (see
579 Sect. 3 and the Supplement), suggests no significant emissions from China.

580 For western Japan we find emissions of ~0.02 Gg yr⁻¹ (no trend), ~30 % lower than the a priori emissions (from Saito
581 et al. 2010, see Sect. 4.4). While total country emissions are likely higher, the available bottom-up information (see
582 Sect. 3 and Supplement) suggests 1 order of magnitude lower emissions for all of Japan. For South Korea, the
583 inversion adjusts emissions down to 0.01–0.02 Gg yr⁻¹ in most years and up to ~0.04 Gg yr⁻¹ in 2014 and 2015.
584 Except perhaps for 2012 and 2017, emissions from South Korea are significantly higher than the 0.003–0.008 Gg yr⁻¹
585 suggested by the available bottom-up information. Emissions from Taiwan show no trend and are relatively small
586 with ~0.01 Gg yr⁻¹, which is ~50 % of ~0.02 Gg yr⁻¹ indicated by the Taiwanese NIR, though it should be noted that
587 the inversion has relatively low sensitivities for some parts of Taiwan (see Fig. S10). Overall, emissions from
588 western Japan, South Korea, and Taiwan are small, despite their large semiconductor industries (see also Fig. 7),
589 suggesting that this industry sector is not a major emitter of *c*-C₄F₈. Emissions from North Korea are also small.

590 Combined regional *c*-C₄F₈ emissions doubled from 2010 to 2016, driven by Chinese emissions. They represent $31 \pm$
591 4 % of global emissions (2010–2017), while eastern China's emissions represent 28 ± 4 %. The difference between
592 global and eastern Asian emissions remained relatively consistent, ranging from ~1.04 Gg yr⁻¹ in 2010 to 1.47 Gg yr⁻¹
593 in 2017 with an average of 1.20 ± 0.14 Gg yr⁻¹ from 2010 to 2017 and 1.15 ± 0.03 Gg yr⁻¹ from 2011 to 2015, the
594 years with the best data coverage at GSN and thus highest confidence in the results. This means that the increase in
595 global emissions is essentially explained by the increase in eastern Asian emissions, i.e. mostly from China, but also
596 that significant emissions of ~1.16 Gg yr⁻¹ exist outside of the investigated region (a fraction of which may stem
597 from industries located in parts of China and perhaps Japan where the inversion has low sensitivity).

598 Figure 7 shows that from 2010 to 2017 emissions in eastern China occur from the highly industrialized provinces
599 Shandong, Tianjin, and parts of Henan and Hebei (south/southwest of Beijing) as well as from Shanghai and
600 neighboring Jiangsu (to the north), Anhui (to the west) and Zhejiang (to the south) in the Yangtze River Delta region.
601 Also shown are locations of potential industrial *c*-C₄F₈ point sources. For South Korea, western Japan and Taiwan,
602 semiconductor fabrication plants do not seem to be dominant *c*-C₄F₈ emitters as they are not co-located with large *c*-
603 C₄F₈ emissions (though the inversion has low sensitivity for eastern Japan, where many more FABS and several
604 PTFE and HCFC-22 plants are located, hence emissions from this region cannot be analyzed).



605 In China, the picture is less clear than in South Korea, Japan and Taiwan, as semiconductor fabrication plants in the
606 Yangtze River Delta region are co-located with strong $c\text{-C}_4\text{F}_8$ emissions, while those near Beijing are not. Many of
607 the potential production facilities of TFE and HFP monomers and PTFE and FEP polymers are co-located with areas
608 where strong $c\text{-C}_4\text{F}_8$ emissions occur. This is consistent with information from the second largest producer of PTFE
609 in China that they do not recover $c\text{-C}_4\text{F}_8$ by-product, but do emit $c\text{-C}_4\text{F}_8$ to the atmosphere (Hu, J., personal
610 communication, 2018). Still, the two facilities north east of Beijing do not seem to emit $c\text{-C}_4\text{F}_8$, perhaps reflecting
611 that some producers minimize $c\text{-C}_4\text{F}_8$ emissions, e.g., to increase yield or to use $c\text{-C}_4\text{F}_8$ for other purposes, such as
612 for the semiconductor industry. Several facilities are also located in provinces for which the inversion has low
613 sensitivity. Most HCFC-22 production facilities are not co-located with strong $c\text{-C}_4\text{F}_8$ emissions, while CHCl_3
614 production facilities tend to be in areas with $c\text{-C}_4\text{F}_8$ emissions. This may reflect that CHCl_3 production has shifted
615 from use as feedstock to produce HCFC-22 for dispersive applications (refrigeration or foam blowing), where no $c\text{-C}_4\text{F}_8$
616 $c\text{-C}_4\text{F}_8$ emissions occur, to production of TFE/HFP/PTFE/FEP via HCFC-22 pyrolysis, where $c\text{-C}_4\text{F}_8$ by-product
617 emissions occur, perhaps at the same or close-by facilities. This would be consistent with the start of the HCFC
618 phase-out for dispersive applications in developing countries mandated by the Montreal Protocol on the Protection of
619 Ozone Layer. Then again, CHCl_3 has other uses, e.g. as solvent (Tsai, 2017), without any potential $c\text{-C}_4\text{F}_8$ emissions.
620 There is no strong correlation between $c\text{-C}_4\text{F}_8$ emissions distribution and population density, e.g. emissions from
621 Henan and Hebei provinces are significantly lower than those from Shandong despite similar total population, which
622 may indicate that combustion of fluoropolymers in waste incineration facilities (Morisaki, 1978; Kannan et al., 2005;
623 van der Walt et al., 2008; Ji et al., 2016; Bezuidenhoudt et al., 2017) is not a dominant source of $c\text{-C}_4\text{F}_8$ emissions.
624 If $c\text{-C}_4\text{F}_8$ emissions in eastern Asia are indeed predominantly associated with TFE/HFP/PTFE/FEP production via
625 the pyrolysis of HCFC-22, $c\text{-C}_4\text{F}_8$ emissions may co-occur with small emissions of HCFC-22, TFE and HFP. CHCl_3
626 and HFC-23 emissions may also co-occur as HCFC-22 is produced from CHCl_3 and HFC-23 is a by-product that in
627 developing countries is probably again vented to the atmosphere since the UNFCCC Clean Development Mechanism
628 (CDM) funding to avoid HFC-23 emissions has expired (Simmonds et al., 2018; Say et al., 2019). While the global
629 atmospheric lifetime of TFE is only ~ 2 days, the lifetime of HFP is ~ 6 days (Acerboni et al., 2001), so that HFP may
630 be detectable near strong emission sources and serve as a sensitive marker for regional TFE/HFP/PTFE/FEP
631 production. After adding HFP to the measurements in late 2018, we find strong HFP pollution events at SDZ which
632 are associated with $c\text{-C}_4\text{F}_8$, CHCl_3 , HCFC-22 and HFC-23 pollution events. HFP pollution events at GSN are much
633 weaker, reflecting the short atmospheric lifetime and the more distant source region, but they are also associated with
634 $c\text{-C}_4\text{F}_8$, CHCl_3 , HCFC-22 and HFC-23 pollution events. At both sites, however, $c\text{-C}_4\text{F}_8$ pollution events also co-
635 occur with enhancements of other anthropogenic compounds which may just point to generally polluted air in the
636 region, so it is difficult to draw definitive conclusions. Still it is clear that HFP is emitted in eastern Asia, likely in
637 China, and HFP as well as $c\text{-C}_4\text{F}_8$ are associated with PTFE/FEP production. Measurements of HFP at SIO and ASA,
638 confirm that it is virtually absent from the global background atmosphere even in urban environments.
639 Overall, the strong $c\text{-C}_4\text{F}_8$ emissions in eastern China and their source regions are consistent with emissions from
640 TFE/HFP/PTFE/FEP production facilities due to little or no recovery or abatement of $c\text{-C}_4\text{F}_8$ by-product and the
641 significant fraction of global PTFE production (53–67 % in 2015) in China (see Table S3).



642 5.3.2 Emissions from North Western Europe

643 Outside of eastern Asia, the TAC station in East Anglia, UK shows by far the most frequent and most pronounced *c*-
644 C₄F₈ pollution events of any AGAGE station, with a few reaching ~5 to 10 ppt above NH background, indicating
645 close-by emissions. Data from the TAC, MHD, JFJ and CMN stations and the InTEM regional inverse method (see
646 Sect. 4.5) were used to estimate emissions from North Western Europe (42° N to 59° N and -11° E to 15° E) based
647 on to the areas of highest sensitivity to the observations (see Fig. S11). Compared to eastern Asia, we find only small
648 emissions of $\sim 0.02 \pm 0.01$ Gg yr⁻¹ (2013–2017) without any significant temporal trend, corresponding to only ~1 %
649 of global emissions, despite an estimated 14 % of global PTFE production in 2015 (see Table S3). The mean
650 distribution of emissions is shown in Fig. 8. As in eastern Asia, most identified semiconductor FABS in Europe are
651 not co-located with *c*-C₄F₈ emission hotspots, except perhaps several FABS in Northern France, the UK, and Ireland.
652 Producers of PTFE and FEP and facility locations in Europe were determined from company websites (3M/Dyneon,
653 AGC/Asahi Glass, Arkema, Chemours/DuPont, Saint-Gobin, Solvay) and the European Pollutant Release and
654 Transfer Register (<https://prtr.eea.europa.eu>), but it is very difficult to determine at which of the many facilities
655 PTFE or FEP are actually produced and thus where *c*-C₄F₈ may be emitted. It seems that several facilities in The
656 Netherlands, Belgium, the UK, France, and Italy which likely produce PTFE are co-located with identified *c*-C₄F₈
657 emission hotspots (Fig. 8). Still, many mismatches exist, reflecting the uncertainties in determining the exact facility
658 locations, the relatively small emission strength and uncertainties of the inversion. As in eastern Asia, there seems to
659 be no correlation with population density, which suggests that waste incineration of fluoropolymers is not a dominant
660 *c*-C₄F₈ source here either. While emissions are relatively small, it is noteworthy that UNFCCC reporting by The
661 Netherlands, the UK, Belgium, and France suggest much smaller *c*-C₄F₈ emissions.

662 5.3.3 Emissions from South Eastern Australia

663 Other urban locations of the AGAGE network, such as SIO, USA and ASA, Australia show much smaller pollution
664 events above global background (up to ~2.5 ppt) than those seen at TAC, suggesting even lower emissions. Still, the
665 few pollution events at ASA and even CGO are interesting as production of PFCs in Australia has never been
666 recorded. CFC-11, CFC-12, and HCFC-22 were manufactured starting in 1962 at two facilities in Sydney, but
667 production ceased in 1995 and trace gas emissions from Sydney are rarely if ever observable at CGO or ASA.
668 Without any currently known fluorocarbon production, any *c*-C₄F₈ pollution events observed at CGO or ASA should
669 not be due to fugitive emissions. *c*-C₄F₈ imports to Australia are ~4 to 50 kg yr⁻¹ (2011–2015), likely for minor
670 refrigeration uses. In contrast, small but identifiable *c*-C₄F₈ pollution episodes at CGO suggest Melbourne emissions
671 of ~2 t yr⁻¹ (0.002 Gg yr⁻¹) in 2016 (down from ~5 t yr⁻¹ in 2009, Inter Species Correlation method, ISC, c.f., Fraser
672 et al., 2014; Dunse et al., 2018). Scaled by population to Australia (for lack of a better proxy), emissions from 2009
673 to 2016 could be ~10–25 t yr⁻¹ (0.01–0.025 Gg yr⁻¹), 2–3 orders of magnitude higher than import data suggests. Since
674 early 2017, HFP has been measured at ASA. Occasional, small HFP pollution events, which are often, but not
675 always, associated with *c*-C₄F₈ pollution events, may point to small scale production of PTFE/FEP/TFE/HFP in
676 Melbourne or perhaps these small emissions stem from incineration of waste containing fluoropolymers. Another
677 possible explanation could be that more *c*-C₄F₈ is imported in products for minor applications than identified in
678 import data due to inadequate labelling. On a global scale, estimated Australian *c*-C₄F₈ emissions of ~0.015 Gg yr⁻¹



679 are small, ~0.7 % of global emissions. PFC (CF₄, C₂F₆) pollution episodes at Cape Grim and Aspendale due to PFC
680 emissions from South Eastern Australian aluminum smelters (Portland and Pt. Henry, Victoria and Bell Bay,
681 Tasmania) do not show any evidence of *c*-C₄F₈ emissions (Fraser et al., 2013; CSIRO unpublished data).

682 **5.3.4 Emissions from undersampled regions such as the US, India, Russia**

683 The AGAGE network does not closely monitor large areas of the globe where *c*-C₄F₈ emissions may occur. For
684 example, many semiconductor FABs are located in the western, southern, and eastern US and chemical facilities
685 located in the southern and eastern US are estimated to account for ~10 % of global PTFE production in 2015, while
686 facilities in India and Russia are estimated to account for ~8 % and ~6 %, respectively (see Tables S3 and S4). The
687 two AGAGE stations in California are only able to capture a fraction of these emissions due to predominant westerly
688 winds and therefore we cannot estimate *c*-C₄F₈ emissions from the continental US. If PTFE production facilities in
689 the US are operated as in NW Europe, emissions should be similarly small. If facilities in India and Russia are
690 operated as in China, emissions could be significant as well. In the case of Russia this seems likely as the original
691 technology for fluoropolymer production in China apparently stems from Russia (Buznik, 2009).

692 **5.3.5 Emissions from India**

693 Say et al. (2019) recently presented measurements from an aircraft campaign in June and July 2016 (see Sect. 2.4)
694 over the Indian subcontinent to determine emissions of ODS and HFCs. Here we use their *c*-C₄F₈ measurements and
695 the NAME-HB inversion (see Sect. 4.6) and estimate emissions of 0.14 (0.09–0.20) Gg yr⁻¹ for Northern and Central
696 India (NCI). Data are only available for two months in 2016, but seasonality in industrial emissions of *c*-C₄F₈ is not
697 expected. The posterior emissions distribution (Fig. 9) is consistent with emissions from facilities producing PTFE.
698 Several of the HCFC-22 production facilities are co-located or very close to these PTFE producing facilities,
699 suggesting that a fraction of HCFC-22 is pyrolyzed to produce monomers for PTFE and FEP. Two HCFC-22
700 production facilities are outside of areas with strong *c*-C₄F₈ emissions, possibly because these two sites focus on
701 production of HCFC-22 for dispersive applications (refrigeration or foam blowing), where no *c*-C₄F₈ emissions
702 occur. The single known FAB in India is not co-located with significant *c*-C₄F₈ emissions. As in eastern Asia and
703 North Western Europe, there is no apparent correlation of *c*-C₄F₈ emissions with population density. Emissions
704 predominantly occur outside of the Indo-Gangetic plain, the most densely populated region of India. The derived
705 emissions account for 6.8 (4.4–9.7) % of global *c*-C₄F₈ emissions in 2016, in comparison to the estimated ~8 % of
706 2015 global PTFE production capacity (see Table S3). Perhaps even clearer than in eastern Asia, these results point
707 to PTFE production as dominant emission source of *c*-C₄F₈. All known Indian PTFE manufacturers are located
708 within the NCI domain, hence the estimated emissions are likely to be roughly representative of India's national total,
709 though further atmospheric measurements would be required to confirm this.

710 **5.3.6 Emissions from facilities in Russia**

711 The ZEP site in remote Svalbard shows ten small *c*-C₄F₈ pollution events above NH background of up to ~0.4 ppt.
712 FLEXPART backward simulations could trace some of these events to two facilities in Russia which produce PTFE
713 and halogenated chemicals including *c*-C₄F₈ itself (HaloPolymer, Kirovo-Chepetsk, Kirov Oblast and Galogen Open



714 Joint-Stock Company, Perm). Figure S12 shows the FLEXPART footprint emission sensitivity map for the largest
715 observed $c\text{-C}_4\text{F}_8$ enhancement on November 19, 2016, suggesting direct transport from the two PTFE production
716 sites. The emission sensitivity maps indicate that for six of the ten observed pollution events the air had clearly
717 passed over one or both of these two sources, even though the timing of the observed events was often not well
718 matched by the model, which was sometimes off by up to about half a day. While this is not surprising given the
719 large distance between the source and the receptor, it means that the two sources could not be clearly separated,
720 especially since the FLEXPART emission sensitivity often also covered both sites for the same arrival times at ZEP.
721 Assuming a unit emission at those two locations and scaling the resulting simulated mole fractions at ZEP to the
722 observed enhancements above background we estimated the emission strength for the two sites together for each
723 event (see Sect. 4.7). Five of the ten pollution events could be approximately reproduced by this method and required
724 a flux of $0.18 \pm 0.06 \text{ Gg yr}^{-1}$, while the sixth event required $\sim 0.54 \text{ Gg yr}^{-1}$. Averaged for all six events $0.24 \pm 0.15 \text{ Gg}$
725 yr^{-1} would be required. Either of these fluxes would be significant, representing $9 \pm 3 \%$, 26% , and $12 \pm 7 \%$ of
726 global emissions, respectively, compared to $\sim 6 \%$ of estimated global PTFE production in Russia. The uncertainty of
727 this estimate is large because only a few events were observed and not all of them were reproduced equally well by
728 FLEXPART. Similar to eastern Asia, the largest $c\text{-C}_4\text{F}_8$ pollution event also showed enhancements of HCFC-22 and
729 HFC-23, pointing to the production of PTFE as source, but other halogenated compounds were also elevated.

730 **6 Summary and conclusions**

731 We determine the atmospheric histories of $c\text{-C}_4\text{F}_8$ (PFC-318, perfluorocyclobutane) in both hemispheres based on
732 measurements of archived, in situ, and firn air samples in conjunction with the CSIRO firn model, the AGAGE 12-
733 box model, and two global inversion frameworks. Compared to previous studies, our work extends the Southern
734 Hemisphere record from 1978 back to 1900 and from 2008 until 2017 and adds a Northern Hemisphere record, all
735 reported with better precisions for air archive measurements ($\sim 1\text{--}2 \%$) and a lower uncertainty (2% versus $\leq 7 \%$) of
736 the SIO-14 gravimetric calibration scale. We find global $c\text{-C}_4\text{F}_8$ atmospheric mole fractions near zero ($< 0.02 \text{ ppt}$)
737 from 1900 until the early 1960s, after which they rose sharply, reaching 0.45 ppt in 1980, 0.74 ppt in 1990, 0.97 ppt
738 in 2000, 1.29 ppt in 2010, and 1.66 ppt in 2017. Global $c\text{-C}_4\text{F}_8$ emissions started to increase in the 1960s from near
739 zero to $\sim 1.2 \text{ Gg yr}^{-1}$ in the late 1970s to the late 1980s. After this, emissions declined to $\sim 0.8 \text{ Gg yr}^{-1}$ in the mid-
740 1990s to early 2000s. After this emissions again increased, reaching $\sim 2.2 \text{ Gg yr}^{-1}$ in 2017. These global emissions are
741 significantly larger than bottom-up inventory information.

742 Using the NAME-HB regional inverse method and observations at Gosan station we find that emissions from eastern
743 Asia rose from $\sim 0.36 \text{ Gg yr}^{-1}$ in 2010 to $\sim 0.73 \text{ Gg yr}^{-1}$ in 2016 and 2017, representing $31 \pm 4 \%$ of global emissions,
744 predominantly from eastern China. Strong $c\text{-C}_4\text{F}_8$ emissions are found from heavily industrialized provinces
745 south/southwest of Beijing and near the Yangtze River Delta. In contrast, emissions from western Japan, South
746 Korea, and Taiwan are small, suggesting that their large semiconductor industries are not major $c\text{-C}_4\text{F}_8$ emitters.
747 Overall, the strong $c\text{-C}_4\text{F}_8$ emissions in eastern China and their spatial pattern are consistent with emissions from
748 production of PTFE and other fluoropolymers. A significant fraction of global PTFE production ($53\text{--}67 \%$ in 2015)



749 occurs in China and, as indicated by the second largest producer of PTFE in China, the $c\text{-C}_4\text{F}_8$ by-product from the
750 underlying HCFC-22 pyrolysis process is not recovered or abated, but rather emitted to the atmosphere.

751 Based on samples collected over the Indian subcontinent in mid-2016, we determine emissions of 0.14 (0.09–0.20)
752 Gg yr^{-1} $c\text{-C}_4\text{F}_8$ from Northern and Central India (NCI), ~6.8 (4.4–9.7) % of global emissions. Even clearer than in
753 China, the determined emission map is consistent with emissions from PTFE production.

754 Using the InTEM regional inverse method and measurements at four western European stations, we only find small
755 NW European emissions of $\sim 0.02 \pm 0.01 \text{ Gg yr}^{-1}$ $c\text{-C}_4\text{F}_8$ from 2013–2017 (~1 % of global emissions), in contrast to
756 an estimate of 14 % of global PTFE production capacity in 2015. The inversion also points to facilities which may
757 produce PTFE and FEP and/or semiconductor fabrication plants though the picture is less clear.

758 No obvious correlation between population density and $c\text{-C}_4\text{F}_8$ emissions is found in Eastern Asia, NCI, and NW
759 Europe, indicating that incineration of waste containing fluoropolymers is not a major source of $c\text{-C}_4\text{F}_8$.

760 Based on data from two Australian stations and an Inter Species Correlation method, Australian $c\text{-C}_4\text{F}_8$ emissions are
761 estimated to be small, perhaps ~0.7 % of global $c\text{-C}_4\text{F}_8$ emissions. We find no evidence for $c\text{-C}_4\text{F}_8$ production from
762 two large aluminum smelters in SE Australia.

763 Based on a few $c\text{-C}_4\text{F}_8$ pollution events observed at Zeppelin station and a rough FLEXPART analysis, we estimate
764 that emissions from two Russian facilities known to produce PTFE and halocarbons including $c\text{-C}_4\text{F}_8$ itself could be
765 $\sim 0.24 \pm 0.15 \text{ Gg yr}^{-1}$. While this could represent significant fraction of global emissions (possibly ranging from 5 to
766 26 %), uncertainties are very large.

767 In summary, for the year 2016, we find global $c\text{-C}_4\text{F}_8$ emissions of $2.06 \pm 0.10 \text{ Gg yr}^{-1}$, with $0.73 \pm 0.12 \text{ Gg yr}^{-1}$ from
768 parts of eastern Asia (36 % of the global total), 0.14 (0.09–0.20) Gg yr^{-1} from Northern and Central India (6.8 %),
769 $\sim 0.02 \pm 0.01 \text{ Gg yr}^{-1}$ from North Western Europe (~1 %), and $\sim 0.015 \text{ Gg yr}^{-1}$ from Australia (~0.7 %).

770 Current monitoring capabilities of the AGAGE network leave large areas with potential $c\text{-C}_4\text{F}_8$ emission sources un-
771 or under monitored, e.g. most of the U.S., India, Russia, western China, and eastern Japan where various
772 semiconductor facilities and fluorochemical and fluoropolymer production plants are located.

773 While many possible uses and emission sources of $c\text{-C}_4\text{F}_8$ are found in the literature, the start of significant $c\text{-C}_4\text{F}_8$
774 emissions around the 1960s may well be related to the initial synthesis of PTFE in 1938 with commercial production
775 of PTFE (“Teflon”) by DuPont commencing in 1947 (Gangal and Brothers, 2015) via pyrolysis of HCFC-22 with $c\text{-C}_4\text{F}_8$
776 as a by-product/intermediate. It seems unlikely that process control or abatement to minimize $c\text{-C}_4\text{F}_8$ by-
777 production were in place in the early decades of PTFE production and $c\text{-C}_4\text{F}_8$ by-product was probably emitted to the
778 atmosphere, explaining the steep increase in global emissions reconstructed here. With the advent of UNFCCC by-
779 product reporting requirements in the 1990s, concern about climate change and product stewardship, abatement, and
780 perhaps collection of $c\text{-C}_4\text{F}_8$ for use in the semiconductor industry where it can be easily abated, it is conceivable that
781 fugitive $c\text{-C}_4\text{F}_8$ in developed countries (UNFCCC Annex 1) overall were reduced, explaining the observed
782 stabilization and reduction of global emissions in the 1980s and 1990s. Similar efforts to contain and destroy by-
783 product emissions of fluorocarbons, e.g. HFCs, from the 1980s to the 2000s are documented in the Toxics Release
784 Inventory (<https://www.epa.gov/toxics-release-inventory-tri-program>) Program of the US EPA and the European
785 Pollutant Release and Transfer Register. Concurrently, production of PTFE in China increased rapidly, e.g. from
786 2000 to 2005 by $\sim 26 \text{ % yr}^{-1}$, followed by a slowdown to $\sim 14 \text{ % yr}^{-1}$ from 2005 to 2015 and perhaps $\sim 8 \text{ % yr}^{-1}$ from



787 2015 onward, reaching an estimated 53–67 % of global production in 2015 (see Tables S2, 3, and 4). Without any
788 emission reduction requirements, it is conceivable that fugitive emissions of *c*-C₄F₈ from PTFE production in China,
789 and other developing (UNFCC non-Annex 1) countries, today dominate global emissions, in agreement with our
790 analysis. The 2010 to 2016 rise in rates of eastern Chinese (eastern Asian) *c*-C₄F₈ emissions of ~15 % yr⁻¹ (~13 % yr⁻¹)
791 determined here are compatible to these PTFE production increase rates of 14 to 8 % yr⁻¹ in China. Barring other
792 developments, we predict that *c*-C₄F₈ emissions will continue to rise and that *c*-C₄F₈ will become the second most
793 important PFC emitted to the global atmosphere in terms of CO₂-equivalent emissions within a year or two. While
794 the 2017 radiative forcing of *c*-C₄F₈ (~0.52 mW m⁻²) is very small compared to that of CO₂, emissions *c*-C₄F₈ and
795 other perfluorinated compounds with similar long lifetimes and high radiative efficiencies essentially permanently
796 alter the radiative budget of Earth. The fact that significant emissions of ~1.16 Gg yr⁻¹ of global emissions (56 %),
797 exist outside of the monitored regions clearly shows that observational capabilities and reporting requirements need
798 to be improved to understand global and country wide emissions of PFCs and other synthetic greenhouse gases and
799 ozone depleting substances.

800 7 Author contributions

801 JM contributed to archive, firm, and in situ measurements, interpreted the data, and prepared the manuscript with
802 contributions from all co-authors. CMT provided CSIRO firm model and CSIRO global inversion results and
803 interpretation. MR provided Bristol global inversion results. LMW provided NAME-HB model runs and emission
804 estimated for East Asia, DS and ALG provided the same for India. AJM and LMW provided InTEM model runs and
805 emissions for Europe. AS and NE provided FLEXPART model runs and guided estimation of Russian emissions. DS
806 and ALG provided the aircraft data from India. CMT, MR, LMW, AJM, DS, ALG, AS, and PJF contributed
807 significantly to the text. LPS, DJI, TA, JM, PJF, PBK provided and oversaw CSIRO air archive and NH archive
808 measurements. MKV, SP, SL, M-KP, COJ, LPS, PBK, SOD, PGS, DY, PBK, KMS, OH, BM, CL, JK, JA, MM, SR,
809 and BY oversaw station operations and provided quality controlled measurement data. PJF provided the estimate of
810 Australian emissions. CMH provided gravimetric calibration and calibration propagation for the whole AGAGE
811 network. PKS wrote the software to run all instruments and analyze all measurement data. MKV, BH, CB, VP,
812 DME, and JS provided firm data and were instrumental in their interpretation. AMcC provided insight into UNFCCC
813 reporting and bottom-up inventories as well as industrial processes. EM and MC greatly helped with the gathering of
814 locations of semiconductor facilities. RGP and RFW provided overall project oversight.

815 8 Acknowledgments

816 Development of the Medusa GC/MS systems, calibrations, and measurements at the Scripps Institution of
817 Oceanography, La Jolla as well as operations of Trinidad Head, CA were carried out as part of the international
818 AGAGE research program and supported by the NASA Upper Atmospheric Research Program in the US with grants
819 NNX07AE89G to MIT, NNX07AF09G and NNX07AE87G to SIO. In the UK, the Department for Business, Energy
820 & Industrial Strategy (BEIS) provided support through contract 1028/06/2015 to the University of Bristol for Mace
821 Head, Ireland, for Tacolneston, UK and to the UK Met Office for InTEM analysis. The National Oceanic and
23



822 Atmospheric Administration (NOAA) in the US provided support to the University of Bristol for operations at
823 Ragged Point, Barbados through contract RA-133-R15-CN-0008 and supported operations at Cape Matatula,
824 American Samoa. Operations in Australia were supported by the Commonwealth Scientific and Industrial Research
825 Organization (CSIRO), the Bureau of Meteorology (Australia), the Department of Environment and Energy
826 (Australia), and Refrigerant Reclaim Australia. Operations at Jungfraujoch were supported by the Swiss National
827 Program HALCLIM (Swiss Federal Office for the Environment, FOEN) and by the International Foundation High
828 Altitude Research Stations Jungfraujoch and Gornergrat (HFSJG). Operations at Zeppelin were supported by the
829 Norwegian Environment Agency. Operations at Monte Cimone were supported by the National Research Council of
830 Italy and the Italian Ministry of Education, University and Research through the Project of National Interest
831 Nextdata. Operations at Gosan were supported by the National Strategic Project-Fine particle of the National
832 Research Foundation of Korea (NRF) funded by the Ministry of Science and ICT (MSIT), the Ministry of
833 Environment (ME), and the Ministry of Health and Welfare(MOHW) (No. NRF-2017M3D8A1092225). Operations
834 at Shangdianzi were supported by the National Nature Science Foundation of China (41575114). We are indebted to
835 the staff and scientists at AGAGE and other sites for their continuing contributions to produce high quality
836 measurements of atmospheric trace gases. Firn air sampling at Law Dome was supported by the Australian Antarctic
837 Division, Australian Antarctic Science Program, and Australia's Nuclear Science and Technology Organisation. We
838 acknowledge the members of the firn air sampling teams at South Pole in 2001 and at NEEM in 2008. Firn air
839 sampling at Summit station was supported through NSF grants ARC-1203779 and ARC-1204084, with airlift
840 support from the 109th New York Air National guard. We thank E. J. Dlugokencky and the National Oceanic and
841 Atmospheric Administration (NOAA) Earth System Research Laboratory (ESRL) Global Monitoring Division
842 (GMD) Carbon Cycle Greenhouse Gases (CCGG) group for measurements which were instrumental for
843 characterizing the Summit13 firn site. We also thank C.D. Keeling (deceased) and R.F. Keeling (SIO) for air
844 samples. We thank Dr. T. Saito for helpful discussions. Matthew Rigby was supported in part by advanced research
845 fellowships from the UK Natural Environment Research Council (NERC, NE/1021365/1). Anita L. Ganesan was
846 funded under a UK Natural Environment Research Council Independent Research Fellowship (NE/L010992/1). We
847 acknowledge the contribution of the UK National Environmental Research Council (NERC), the Ministry of Earth
848 Sciences, Government of India and the Principal Investigators of 'Drivers of the South Asian Monsoon' aircraft
849 campaign in India. Funding for the measurements used here were made possible by NERC grant NE/I027282/1.

850 **References**

- 851 Acerboni, G., Beukes, J. A., Jensen, N. R., Hjorth, J., Myhre, G., Nielsen, C. J., and Sundet, J. K.:
852 Atmospheric degradation and global warming potentials of three perfluoroalkenes, *Atmos.*
853 *Environ.*, 35, 24, 4113-4123, 10.1016/S1352-2310(01)00209-6, 2001.
- 854 Adolph, A. C., and Albert, M. R.: Gas diffusivity and permeability through the firn column at
855 Summit, Greenland: measurements and comparison to microstructural properties, *The*
856 *Cryosphere*, 8, 1, 319-328, 10.5194/tc-8-319-2014, 2014.
- 857 Arnold, T., Mühle, J., Salameh, P. K., Harth, C. M., Ivy, D. J., and Weiss, R. F.: Automated
858 measurement of nitrogen trifluoride in ambient air, *Anal. Chem.*, 84, 11, 4798–4804,
859 10.1021/ac300373e, 2012.
- 860 Arnold, T., Manning, A. J., Kim, J., Li, S., Webster, H., Thomson, D., Mühle, J., Weiss, R. F.,
861 Park, S., and O'Doherty, S.: Inverse modelling of CF₄ and NF₃ emissions in East Asia, *Atmos.*
862 *Chem. Phys.*, 18, 18, 13305-13320, 10.5194/acp-18-13305-2018, 2018.
- 863 Aydin, M., Saltzman, E. S., De Bruyn, W. J., Montzka, S. A., Butler, J. H., and Battle, M.:
864 Atmospheric variability of methyl chloride during the last 300 years from an Antarctic ice core
865 and firn air, *Geophys. Res. Lett.*, 31, 2, L02109, 10.1029/2003GL018750, 2004.
- 866 Battle, M., Bender, M., Sowers, T., Tans, P. P., Butler, J. H., Elkins, J. W., Ellis, J. T., Conway,
867 T., Zhang, N., Lang, P., and Clarke, A. D.: Atmospheric gas concentrations over the past century
868 measured in air from firn at the South Pole, *Nature*, 383, 6597, 231-235, 1996.
- 869 Bezuidenhoudt, A., Sonnendecker, P. W., and Crouse, P. L.: Temperature and pressure effects on
870 the product distribution of PTFE pyrolysis by means of qualitative, in-line FTIR analysis, *Polym.*
871 *Degrad. Stab.*, 142, 79-88, 10.1016/j.polymdegradstab.2017.05.025, 2017.
- 872 Broyer, E., Bekker, A. Y., and Ritter, A. B.: Kinetics of the pyrolysis of chlorodifluoromethane,
873 *Ind. Eng. Chem. Res.*, 27, 1, 208-211, 10.1021/ie00073a039, 1988.
- 874 Buizert, C., Martinerie, P., Petrenko, V. V., Severinghaus, J. P., Trudinger, C. M., Witrant, E.,
875 Rosen, J. L., Orsi, A. J., Rubino, M., Etheridge, D. M., Steele, L. P., Hogan, C., Laube, J. C.,
876 Sturges, W. T., Levchenko, V. A., Smith, A. M., Levin, I., Conway, T. J., Dlugokencky, E. J.,
877 Lang, P. M., Kawamura, K., Jenk, T. M., White, J. W. C., Sowers, T., Schwander, J., and Blunier,
878 T.: Gas transport in firn: multiple-tracer characterisation and model intercomparison for NEEM,
879 Northern Greenland, *Atmos. Chem. Phys.*, 12, 9, 4259-4277, 10.5194/acp-12-4259-2012, 2012.
- 880 Buznik, V. M.: Fluoropolymer chemistry in Russia: Current situation and prospects, *Russ. J. Gen.*
881 *Chem.*, 79, 3, 520-526, 10.1134/s1070363209030335, 2009.
- 882 Cai, B., Liu, H., Kou, F., Yang, Y., Yao, B., Chen, X., Wong, D. S., Zhang, L., Li, J., Kuang, G.,
883 Chen, L., Zheng, J., Guan, D., and Shan, Y.: Estimating perfluorocarbon emission factors for
884 industrial rare earth metal electrolysis, *Resources, Conservation and Recycling*, 136, 315-323,
885 10.1016/j.resconrec.2018.04.018, 2018.



- 886 Chinoy, P. B., and Sunavala, P. D.: Thermodynamics and kinetics for the manufacture of
887 tetrafluoroethylene by the pyrolysis of chlorodifluoromethane, *Ind. Eng. Chem. Res.*, 26, 7, 1340-
888 1344, 10.1021/ie00067a013, 1987.
- 889 Christophorou, L. G., and Olthoff, J. K.: Electron interactions with $c\text{-C}_4\text{F}_8$, *J. Phys. Chem. Ref.*
890 *Data*, 30, 2, 449-473, 2001.
- 891 Chung, M. O., and Bai, C.: Thermodynamic property variation of nonazeotropic refrigerant
892 mixtures (NARMs) in the temperature gliding zone, *Chemical Engineering Communications*,
893 180, 1, 1-17, 10.1080/00986440008912199, 2000.
- 894 Cunnold, D. M., Prinn, R. G., Rasmussen, R. A., Simmonds, P. G., Alyea, F. N., Cardelino, C.
895 A., Crawford, A. J., Fraser, P. J., and Rosen, R. D.: The Atmospheric Lifetime Experiment, 3.
896 Lifetime Methodology and Application to 3 Years of CFCl_3 Data, *J. Geophys. Res.*, 88, C13,
897 8379-8400, 1983.
- 898 Cunnold, D. M., Weiss, R. F., Prinn, R. G., Hartley, D., Simmonds, P. G., Fraser, P. J., Miller, B.,
899 Alyea, F. N., and Porter, L.: GAGE/AGAGE measurements indicating reductions in global
900 emissions of CCl_3F and CCl_2F_2 in 1992-1994, *J. Geophys. Res.*, 102, D1, 1259-1269, 1997.
- 901 Cunnold, D. M., Steele, L. P., Fraser, P. J., Simmonds, P. G., Prinn, R. G., Weiss, R. F., Porter, L.
902 W., O'Doherty, S., Langenfelds, R. L., Krummel, P. B., Wang, H. J., Emmons, L., Tie, X. X., and
903 Dlugokencky, E. J.: In situ measurements of atmospheric methane at GAGE/AGAGE sites during
904 1985-2000 and resulting source inferences, *J. Geophys. Res.*, 107, D14, 10.1029/2001JD001226,
905 2002.
- 906 Dunse, B. L., Derek, N., Fraser, P. J., Krummel, P. B., and Steele, L. P.: Australian and global
907 HFC, PFC, sulfur hexafluoride nitrogen trifluoride and sulfuryl fluoride emissions, Report
908 prepared for Australian Government Department of the Environment and Energy, CSIRO Oceans
909 and Atmosphere, Aspendale, Australia, iv, 33 pp.
910 <http://www.environment.gov.au/protection/ozone/publications/csiro-report-australian-global-sgg>,
911 2018.
- 912 EDGAR: European Commission, Joint Research Centre (JRC)/PBL Netherlands Environmental
913 Assessment Agency. Emission Database for Global Atmospheric Research (EDGAR), release
914 version 4.2. <http://edgar.jrc.ec.europa.eu>, 2010.
- 915 Engel, A., M. Rigby (Lead Authors), Burkholder, J. B., Fernandez, R. P., Froidevaux, L., Hall, B.
916 D., Hossaini, R., Saito, T., Vollmer, M. K., B. Yao (Coauthors), Altas, E., Bernath, P., Blake, D.
917 R., Dutton, G., Krummel, P., Laube, J. C., Mahieu, E., Montzka, S. A., Mühle, J., Nedoluha, G.,
918 O'Doherty, S. J., Oram, D. E., Pfeilsticker, K., Prinn, R. G., Quack, B., Simpson, I. J., R.F. Weiss
919 (Contributors), Liang, Q., and S. Reimann (Review Editors): Update on Ozone-Depleting
920 Substances (ODSs) and Other Gases of Interest to the Montreal Protocol (Chapter 1), in:
921 Scientific Assessment of Ozone Depletion: 2018, Global Ozone Research and Monitoring
922 Project–Report No. 58, World Meteorological Organization, Geneva, Switzerland, 2018.
- 923 Fraser, P., Steele, P., and Cooksey, M.: PFC and Carbon Dioxide Emissions from an Australian
924 Aluminium Smelter Using Time-Integrated Stack Sampling and GC-MS, GC-FID Analysis, in:
925 Light Metals 2013, John Wiley & Sons, Inc., 871-876, 2013.



- 926 Fraser, P. J., Dunse, B. L., Manning, A. J., Walsh, S., Wang, R. H. J., Krummel, P. B., Steele, L.
927 P., Porter, L. W., Allison, C., O'Doherty, S., Simmonds, P. G., Mühle, J., Weiss, R. F., and Prinn,
928 R. G.: Australian carbon tetrachloride emissions in a global context, *Environ. Chem.*, 11, 1, 77-
929 88, 10.1071/EN13171, 2014.
- 930 Fuller, E. N., Schettler, P. D., and Giddings, J. C.: A new method for prediction of binary gas-
931 phase diffusion coefficients, *Industrial & Engineering Chemistry*, 58, 5, 18-27,
932 10.1021/ie50677a007, 1966.
- 933 Ganesan, A. L., Rigby, M., Zammit-Mangion, A., Manning, A. J., Prinn, R. G., Fraser, P. J.,
934 Harth, C. M., Kim, K. R., Krummel, P. B., Li, S., Mühle, J., O'Doherty, S. J., Park, S., Salameh,
935 P. K., Steele, L. P., and Weiss, R. F.: Characterization of uncertainties in atmospheric trace gas
936 inversions using hierarchical Bayesian methods, *Atmos. Chem. Phys.*, 14, 8, 3855-3864,
937 10.5194/acp-14-3855-2014, 2014.
- 938 Gangal, S. V., and Brothers, P. D.: Perfluorinated Polymers, in: *Kirk-Othmer Encyclopedia of*
939 *Chemical Technology*, 2015.
- 940 Harnisch, J., Wing, I. S., Jacoby, H. D., and Prinn, R. G.: Primary Aluminum Production: Climate
941 Policy, Emissions and Costs, Massachusetts Institute of Technology, Report #44, 1998.
- 942 Harnisch, J.: Reactive Fluorine Compounds, in: *Reactive Halogen Compounds in the Atmosphere*
943 *Vol. 4 Part E, The Handbook of Environmental Chemistry*, Springer Berlin/Heidelberg, 81-111,
944 1999.
- 945 Harnisch, J.: Atmospheric perfluorocarbons: sources and concentrations, in: *Non-CO₂ greenhouse*
946 *gases: scientific understanding, control and implementation*, edited by: Ham, J. v., Baede, A.,
947 Meyer, L., and Ybema, R., Kluwer Academic Publishers, Netherlands, 205-210, 2000.
- 948 Hastings, W. K.: Monte Carlo sampling methods using Markov chains and their applications,
949 *Biometrika*, 57, 1, 97-109, 10.1093/biomet/57.1.97, 1970.
- 950 Holliday, R. D., and Henry, J. L.: Anode polarization fluorocarbon formation in aluminum
951 reduction cells, *J. Ind. Eng. Chem.*, 51, 10, 1289-1292, 1959.
- 952 IPCC: 2006 IPCC Guidelines for National Greenhouse Gas Inventories, Prepared by the National
953 Greenhouse Gas Inventories Programme, 2006.
- 954 Ivy, D. J., Arnold, T., Harth, C. M., Steele, L. P., Mühle, J., Rigby, M., Salameh, P. K., Leist, M.,
955 Krummel, P. B., Fraser, P. J., Weiss, R. F., and Prinn, R. G.: Atmospheric histories and growth
956 trends of C₄F₁₀, C₅F₁₂, C₆F₁₄, C₇F₁₆ and C₈F₁₈, *Atmos. Chem. Phys.*, 12, 9, 4313-4325,
957 10.5194/acp-12-4313-2012, 2012.
- 958 Ji, L., Lu, S., Yang, J., Du, C., Chen, Z., Buekens, A., and Yan, J.: Municipal solid waste
959 incineration in China and the issue of acidification: A review, *Waste Management & Research*,
960 34, 4, 280-297, 10.1177/0734242x16633776, 2016.



- 961 Jianming, S.: Synthesis of Hexafluoropropene by Co-pyrolysis Reaction of Tetrafluoroethylene
962 with Octafluorocyclobutane, Masters Degree, Department of Chemical Engineering, Zhajiang
963 University, Hangzhou, China, 2006.
- 964 Jones, A. R., Thomson, D. J., Hort, M., and Devenish, B.: The UK Met Office's next-generation
965 atmospheric dispersion model, NAME III, in: Air Pollution Modelling and Its Application XVII,
966 edited by: Borrego, C., and Norman, A.-L., 580-589, 2007.
- 967 Kannan, G. K., Gupta, M., and Chandra Kapoor, J.: Estimation of gaseous products and
968 particulate matter emission from garden biomass combustion in a simulation fire test chamber,
969 Atmos. Environ., 39, 3, 563-573, 2005.
- 970 Kass, W.: Tracing Technique in Geohydrology, CRC Press, 1998.
- 971 Kim, J. H., Oh, C. H., Lee, N. E., and Yeom, G. Y.: Effect of N₂O to C₄F₈/O₂ on global warming
972 during silicon nitride plasma enhanced chemical vapor deposition (PECVD) chamber cleaning
973 using a remote inductively coupled plasma source, Jpn. J. Appl. Phys. Part 2 - Lett., 41, 12B,
974 L1495-L1498, 10.1143/jjap.41.11495, 2002.
- 975 Kokkoris, G., Goodyear, A., Cooke, M., and Gogolides, E.: A global model for C₄F₈ plasmas
976 coupling gas phase and wall surface reaction kinetics, J. Phys. D: Appl. Phys., 41, 19, 195211,
977 10.1088/0022-3727/41/19/195211, 2008.
- 978 Langenfelds, R. L., Krummel, P. B., Fraser, P. J., Steele, L. P., Ward, J., and Somerville, N. T.:
979 Archiving of Cape Grim air, Baseline Atmospheric Program Australia 2009-2010, Melbourne,
980 Australia, 2014, edited by: Derek, N., Krummel, P. B., and Cleland, S. J., pp. 44-45, Australian
981 Bureau of Meteorology and CSIRO Marine and Atmospheric Research.
- 982 Lewis, R. J., Sr.: Food additives handbook, Chapman & Hall, New York, 1989.
- 983 Liu, X., Wang, J., Wang, Y., Zhang, Z., and Xiao, D.: Analysis of the insulation characteristics of
984 c-C₄F₈/CO₂ gas mixtures by the Monte Carlo method, Journal of Physics D: Applied Physics, 41,
985 1, 015206, 2008.
- 986 Lovelock, J. E.: Atmospheric Fluorine Compounds as Indicators of Air Movements, Nature, 230,
987 5293, 379-&, 1971.
- 988 Lunt, M. F., Rigby, M., Ganesan, A. L., and Manning, A. J.: Estimation of trace gas fluxes with
989 objectively determined basis functions using reversible-jump Markov chain Monte Carlo, Geosci.
990 Model Dev., 9, 9, 3213-3229, 10.5194/gmd-9-3213-2016, 2016.
- 991 Mackay, D., Shiu, W. Y., Ma, K. C., and Lee, S.: Handbook of Physical-Chemical Properties and
992 Environmental Fate for Organic Chemicals, 2006.
- 993 Maione, M., Giostra, U., Arduini, J., Furlani, F., Graziosi, F., Lo Vullo, E., and Bonasoni, P.: Ten
994 years of continuous observations of stratospheric ozone depleting gases at Monte Cimone (Italy)
995 — Comments on the effectiveness of the Montreal Protocol from a regional perspective, Sci.
996 Total Environ., 445-446, 155-164, 10.1016/j.scitotenv.2012.12.056, 2013.



- 997 Matsunaga, N., Hori, M., and Nagashima, A.: Mutual diffusion coefficients of halogenated-
998 hydrocarbon refrigerant-air systems, *High Temp.-High Press*, 25, 63-70, 1993.
- 999 Matsunaga, N., Hori, M., and Nagashima, A.: Measurements of the mutual diffusion coefficients
1000 of gases by the Taylor method, 7th report, measurements on the SF₆-air, SF₆-N₂, SF₆-O₂, CFC12-
1001 N₂, CFC12-O₂, HCFC22-N₂ and HCFC22-O₂ systems, *Trans. Jpn. Soc. Mech. Eng. B.*, 68, 550-
1002 555, 2002.
- 1003 Matsunaga, N., Hori, M., and Nagashima, A.: Measurements of the mutual diffusion coefficients
1004 of carbon tetrafluoride and methyl bromide in air, nitrogen and oxygen, *Proc. 26th Jpn. Symp.*
1005 *Therm. Props*, 26, 499-501, 2005.
- 1006 Metropolis, N., Rosenbluth, A. W., Rosenbluth, M. N., Teller, A. H., and Teller, E.: Equation of
1007 State Calculations by Fast Computing Machines, *J. Chem. Phys.*, 21, 6, 1087-1092,
1008 10.1063/1.1699114, 1953.
- 1009 Miller, B. R., Weiss, R. F., Salameh, P. K., Tanhua, T., Grealley, B. R., Mühle, J., and Simmonds,
1010 P. G.: Medusa: A sample preconcentration and GC/MS detector system for in situ measurements
1011 of atmospheric trace halocarbons, hydrocarbons, and sulfur compounds, *Anal. Chem.*, 80, 5,
1012 1536-1545, 10.1021/ac702084k, 2008.
- 1013 Morisaki, S.: Simultaneous thermogravimetry-mass spectrometry and pyrolysis--gas
1014 chromatography of fluorocarbon polymers, *Thermochimica Acta*, 25, 2, 171-183, 1978.
- 1015 Morris, R. A., Miller, T. M., Viggiano, A. A., Paulson, J. F., Solomon, S., and Reid, G.: Effects
1016 of electron and ion reactions on atmospheric lifetimes of fully fluorinated compounds, *J.*
1017 *Geophys. Res.*, 100, D1, 1287-1294, 1995.
- 1018 Mühle, J., Ganesan, A. L., Miller, B. R., Salameh, P. K., Harth, C. M., Grealley, B. R., Rigby, M.,
1019 Porter, L. W., Steele, L. P., Trudinger, C. M., Krummel, P. B., O'Doherty, S., Fraser, P. J.,
1020 Simmonds, P. G., Prinn, R. G., and Weiss, R. F.: Perfluorocarbons in the global atmosphere:
1021 tetrafluoromethane, hexafluoroethane, and octafluoropropane, *Atmos. Chem. Phys.*, 10, 11, 5145-
1022 5164, 10.5194/acp-10-5145-2010, 2010.
- 1023 Myhre, G., D. Shindell (Coordinating Lead Authors), Bréon, F.-M., Collins, W., Fuglestedt, J.,
1024 Huang, J., Koch, D., Lamarque, J.-F., Lee, D., Mendoza, B., Nakajima, T., Robock, A., Stephens,
1025 G., Takemura, T., and Zhang, H.: Anthropogenic and Natural Radiative Forcing, in: *Climate*
1026 *Change 2013: The Physical Science Basis. Contribution of Working Group I to the Fifth*
1027 *Assessment Report of the Intergovernmental Panel on Climate Change, Chapter 8*, edited by:
1028 Stocker, T. F., Qin, D., Plattner, G.-K., Tignor, M., Allen, S. K., Boschung, J., Nauels, A., Xia,
1029 Y., Bex, V., and Midgley, P. M., Cambridge University Press, Cambridge, United Kingdom and
1030 New York, NY, USA, 2013.
- 1031 O'Doherty, S., Simmonds, P. G., Cunnold, D. M., Wang, H. J., Sturrock, G. A., Fraser, P. J.,
1032 Ryall, D., Derwent, R. G., Weiss, R. F., Salameh, P., Miller, B. R., and Prinn, R. G.: In situ
1033 chloroform measurements at Advanced Global Atmospheric Gases Experiment atmospheric
1034 research stations from 1994 to 1998, *J. Geophys. Res.*, 106, D17, 20429-20444, 2001.



- 1035 O'Doherty, S., Rigby, M., Mühle, J., Ivy, D. J., Miller, B. R., Young, D., Simmonds, P. G.,
1036 Reimann, S., Vollmer, M. K., Krummel, P. B., Fraser, P. J., Steele, L. P., Dunse, B., Salameh, P.
1037 K., Harth, C. M., Arnold, T., Weiss, R. F., Kim, J., Park, S., Li, S., Lunder, C., Hermansen, O.,
1038 Schmidbauer, N., Zhou, L. X., Yao, B., Wang, R. H. J., Manning, A. J., and Prinn, R. G.: Global
1039 emissions of HFC-143a (CH_3CF_3) and HFC-32 (CH_2F_2) from in situ and air archive atmospheric
1040 observations, *Atmos. Chem. Phys.*, 14, 17, 9249-9258, 10.5194/acp-14-9249-2014, 2014.
- 1041 Oram, D.: Trends of long-lived anthropogenic halocarbons in the Southern Hemisphere and
1042 model calculations of global emissions, P.D. thesis, University of East Anglia, Norwich, U.K.,
1043 1999.
- 1044 Oram, D. E., Mani, F. S., Laube, J. C., Newland, M. J., Reeves, C. E., Sturges, W. T., Penkett, S.
1045 A., Brenninkmeijer, C. A. M., Röckmann, T., and Fraser, P. J.: Long-term tropospheric trend of
1046 octafluorocyclobutane ($\text{c-C}_4\text{F}_8$ or PFC-318), *Atmos. Chem. Phys.*, 12, 1, 261-269, 10.5194/acp-
1047 12-261-2012, 2012.
- 1048 Prinn, R. G., Weiss, R. F., Fraser, P. J., Simmonds, P. G., Cunnold, D. M., Alyea, F. N.,
1049 O'Doherty, S., Salameh, P., Miller, B. R., Huang, J., Wang, R. H. J., Hartley, D. E., Harth, C.,
1050 Steele, L. P., Sturrock, G., Midgley, P. M., and McCulloch, A.: A history of chemically and
1051 radiatively important gases in air deduced from ALE/GAGE/AGAGE, *J. Geophys. Res.*, 105,
1052 D14, 17751-17792, 10.1029/2000jd900141, 2000.
- 1053 Prinn, R. G., Huang, J., Weiss, R. F., Cunnold, D. M., Fraser, P. J., Simmonds, P. G., McCulloch,
1054 A., Harth, C., Salameh, P., O'Doherty, S., Wang, R. H. J., Porter, L., and Miller, B. R.: Evidence
1055 for substantial variations of atmospheric hydroxyl radicals in the past two decades, *Science*, 292,
1056 5523, 1882-1888, 2001.
- 1057 Prinn, R. G., Weiss, R. F., Arduini, J., Arnold, T., DeWitt, H. L., Fraser, P. J., Ganesan, A. L.,
1058 Gasore, J., Harth, C. M., Hermansen, O., Kim, J., Krummel, P. B., Li, S., Loh, Z. M., Lunder, C.
1059 R., Maione, M., Manning, A. J., Miller, B. R., Mitrevski, B., Mühle, J., O'Doherty, S., Park, S.,
1060 Reimann, S., Rigby, M., Saito, T., Salameh, P. K., Schmidt, R., Simmonds, P. G., Steele, L. P.,
1061 Vollmer, M. K., Wang, R. H., Yao, B., Yokouchi, Y., Young, D., and Zhou, L.: History of
1062 chemically and radiatively important atmospheric gases from the Advanced Global Atmospheric
1063 Gases Experiment (AGAGE), *Earth Syst. Sci. Data*, 10, 2, 985-1018, 10.5194/essd-10-985-2018,
1064 2018.
- 1065 Raju, R., Kudo, D., Kubo, Y., Inaba, T., and Shindo, H.: Warming potential reduction of C_4F_8
1066 using inductively coupled plasma, *Japanese Journal of Applied Physics Part 1-Regular Papers*
1067 *Short Notes & Review Papers*, 42, 1, 280-285, 10.1143/jjap.42.280, 2003.
- 1068 Ravishankara, A. R., Solomon, S., Turnipseed, A. A., and Warren, R. F.: Atmospheric lifetimes
1069 of long-lived halogenated species, *Science*, 259, 5092, 194-199, 1993.
- 1070 Rigby, M., Ganesan, A. L., and Prinn, R. G.: Deriving emissions time series from sparse
1071 atmospheric mole fractions, *J. Geophys. Res.*, 116, D8, D08306, 10.1029/2010jd015401, 2011.
- 1072 Rigby, M., Prinn, R. G., O'Doherty, S., Montzka, S. A., McCulloch, A., Harth, C. M., Mühle, J.,
1073 Salameh, P. K., Weiss, R. F., Young, D., Simmonds, P. G., Hall, B. D., Dutton, G. S., Nance, D.,
1074 Mondeel, D. J., Elkins, J. W., Krummel, P. B., Steele, L. P., and Fraser, P. J.: Re-evaluation of



- 1075 the lifetimes of the major CFCs and CH_3CCl_3 using atmospheric trends, *Atmos. Chem. Phys.*, 13,
1076 5, 2691-2702, [10.5194/acp-13-2691-2013](https://doi.org/10.5194/acp-13-2691-2013), 2013.
- 1077 Rigby, M., Prinn, R. G., O'Doherty, S., Miller, B. R., Ivy, D., Mühle, J., Harth, C. M., Salameh,
1078 P. K., Arnold, T., Weiss, R. F., Krummel, P. B., Steele, L. P., Fraser, P. J., Young, D., and
1079 Simmonds, P. G.: Recent and future trends in synthetic greenhouse gas radiative forcing,
1080 *Geophys. Res. Lett.*, 41, 7, 2623-2630, [10.1002/2013gl059099](https://doi.org/10.1002/2013gl059099), 2014.
- 1081 Saito, T., Yokouchi, Y., Stohl, A., Taguchi, S., and Mukai, H.: Large emissions of
1082 perfluorocarbons in East Asia deduced from continuous atmospheric measurements, *Environ. Sci.*
1083 *Technol.*, 44, 11, 4089-4095, [10.1021/es1001488](https://doi.org/10.1021/es1001488), 2010.
- 1084 Sasaki, K., Kawai, Y., Suzuki, C., and Kadota, K.: Absolute density and reaction kinetics of
1085 fluorine atoms in high-density $\text{c-C}_4\text{F}_8$ plasmas, *Journal of Applied Physics*, 83, 12, 7482-7487,
1086 1998.
- 1087 Say, D., Ganesan, A. L., Lunt, M. F., Rigby, M., O'Doherty, S., Harth, C., Manning, A. J.,
1088 Krummel, P. B., and Bauguitte, S.: Emissions of CFCs, HCFCs and HFCs from India, *Atmos.*
1089 *Chem. Phys. Discuss.*, 2019, 1-30, [10.5194/acp-2018-1146](https://doi.org/10.5194/acp-2018-1146), 2019.
- 1090 Siegemund, G., Schwertfeger, W., Feiring, A., Smart, B., Behr, F., Vogel, H., McKusick, B., and
1091 Kirsch, P.: Fluorine Compounds, Organic, in: *Ullmann's Encyclopedia of Industrial Chemistry*,
1092 2016.
- 1093 Simmonds, P. G., Rigby, M., McCulloch, A., Vollmer, M. K., Henne, S., Mühle, J., O'Doherty,
1094 S., Manning, A. J., Krummel, P. B., Fraser, P. J., Young, D., Weiss, R. F., Salameh, P. K., Harth,
1095 C. M., Reimann, S., Trudinger, C. M., Steele, P., Wang, R. H. J., Ivy, D. J., Prinn, R. G.,
1096 Mitrevski, B., and Etheridge, D. M.: Recent increases in the atmospheric growth rate and
1097 emissions of HFC-23 (CHF_3) and the link to HCFC-22 (CHClF_2) production, *Atmos. Chem.*
1098 *Phys.*, 18, 6, 4153-4169, [10.5194/acp-18-4153-2018](https://doi.org/10.5194/acp-18-4153-2018), 2018.
- 1099 Smith, A. M., Levchenko, V. A., Etheridge, D. M., Lowe, D. C., Hua, Q., Trudinger, C. M.,
1100 Zoppi, U., and Elcheikh, A.: In search of in-situ radiocarbon in Law Dome ice and firn, *Nuclear*
1101 *Instruments and Methods in Physics Research Section B: Beam Interactions with Materials and*
1102 *Atoms*, 172, 1-4, 610-622, [10.1016/S0168-583X\(00\)00280-9](https://doi.org/10.1016/S0168-583X(00)00280-9), 2000.
- 1103 Sowers, T., Bernard, S., Aballain, O., Chappellaz, J., Barnola, J.-M., and Marik, T.: Records of
1104 the $\delta^{13}\text{C}$ of atmospheric CH_4 over the last 2 centuries as recorded in Antarctic snow and ice,
1105 *Global Biogeochem. Cycles*, 19, GB2002, [10.1029/2004GB002408](https://doi.org/10.1029/2004GB002408), 2005.
- 1106 Stanley, K. M., Grant, A., O'Doherty, S., Young, D., Manning, A. J., Stavert, A. R., Spain, T. G.,
1107 Salameh, P. K., Harth, C. M., Simmonds, P. G., Sturges, W. T., Oram, D. E., and Derwent, R. G.:
1108 Greenhouse gas measurements from a UK network of tall towers: technical description and first
1109 results, *Atmos. Meas. Tech.*, 11, 3, 1437-1458, [10.5194/amt-11-1437-2018](https://doi.org/10.5194/amt-11-1437-2018), 2018.
- 1110 Stohl, A., Forster, C., Frank, A., Seibert, P., and Wotawa, G.: Technical note: The Lagrangian
1111 particle dispersion model FLEXPART version 6.2, *Atmos. Chem. Phys.*, 5, 2461-2474, 2005.



- 1112 Stohl, A., Seibert, P., Arduini, J., Eckhardt, S., Fraser, P., Grealley, B. R., Lunder, C., Maione, M.,
1113 Mühle, J., O'Doherty, S., Prinn, R. G., Reimann, S., Saito, T., Schmidbauer, N., Simmonds, P.
1114 G., Vollmer, M. K., Weiss, R. F., and Yokouchi, Y.: An analytical inversion method for
1115 determining regional and global emissions of greenhouse gases: Sensitivity studies and
1116 application to halocarbons, *Atmos. Chem. Phys.*, 9, 5, 1597-1620, 2009.
- 1117 Sturges, W. T., Penkett, S. A., Lee, J. M., and Sturges, K. E.: Stratospheric distribution and
1118 lifetime of halogenated hydrocarbons; Final report to the European Commission, Contract EV5V-
1119 CT92-0078, University of East Anglia, Norwich, 1995.
- 1120 Sturges, W. T., Oram, D. E., Penkett, S. A., Fraser, P. J., and Engel, A.: Long-lived halogenated
1121 compounds in the stratosphere, in: *Non-CO₂ Greenhouse Gases: Scientific Understanding,
1122 Control, and Implementation*, edited by: van Ham, J., Baede, A. P. M., Meyer, L. A., and Ybema,
1123 R., Kluwer Academic Publishers, The Netherlands, 239-240, 2000.
- 1124 Sturrock, G. A., Etheridge, D. M., Trudinger, C. M., Fraser, P. J., and Smith, A. M.: Atmospheric
1125 histories of halocarbons from analysis of Antarctic firn air: Major Montreal Protocol species, *J.
1126 Geophys. Res.*, 107, D24, 4765, 10.1029/2002JD002548, 2002.
- 1127 Tabereaux, A. T.: Anode Effects, PFCs, Global Warming, and the Aluminum-Industry, *J. Miner.
1128 Met. Mater. Soc.*, 46, 11, 30-34, 1994.
- 1129 Travnicek, W.: A study of light halogenated hydrocarbons in stratospheric air samples using CG-
1130 MS, diploma thesis, Dept. Jülich, Fachhochschule Aachen, Germany, Aachen, 1998.
- 1131 Trudinger, C. M., Enting, I. G., Etheridge, D. M., Francey, R. J., Levchenko, V. A., Steele, L. P.,
1132 Raynaud, D., and Arnaud, L.: Modeling air movement and bubble trapping in firn, *J. Geophys.
1133 Res.*, 102, D6, 6747-6763, 10.1029/96jd03382, 1997.
- 1134 Trudinger, C. M., Etheridge, D. M., Rayner, P. J., Enting, I. G., Sturrock, G. A., and Langenfelds,
1135 R. L.: Reconstructing atmospheric histories from measurements of air composition in firn, *J.
1136 Geophys. Res.*, 107, D24, 4780, 10.1029/2002JD002545, 2002.
- 1137 Trudinger, C. M., Enting, I. G., Rayner, P. J., Etheridge, D. M., Buizert, C., Rubino, M.,
1138 Krummel, P. B., and Blunier, T.: How well do different tracers constrain the firn diffusivity
1139 profile?, *Atmos. Chem. Phys.*, 13, 3, 1485-1510, 10.5194/acp-13-1485-2013, 2013.
- 1140 Trudinger, C. M., Fraser, P. J., Etheridge, D. M., Sturges, W. T., Vollmer, M. K., Rigby, M.,
1141 Martinerie, P., Mühle, J., Worton, D. R., Krummel, P. B., Steele, L. P., Miller, B. R., Laube, J.,
1142 Mani, F. S., Rayner, P. J., Harth, C. M., Witrant, E., Blunier, T., Schwander, J., O'Doherty, S.,
1143 and Battle, M.: Atmospheric abundance and global emissions of perfluorocarbons CF₄, C₂F₆ and
1144 C₃F₈ since 1800 inferred from ice core, firn, air archive and in situ measurements, *Atmos. Chem.
1145 Phys.*, 16, 18, 11733-11754, 10.5194/acp-16-11733-2016, 2016.
- 1146 Tsai, W. T.: Fate of Chloromethanes in the Atmospheric Environment: Implications for Human
1147 Health, Ozone Formation and Depletion, and Global Warming Impacts, *Toxics*, 5, 4,
1148 10.3390/toxics5040023, 2017.



- 1149 National Inventory Submissions 2016: <https://unfccc.int/process/transparency-and-reporting/reporting-and-review-under-the-convention/greenhouse-gas-inventories/submissions-of-annual-greenhouse-gas-inventories-for-2017/submissions-of-annual-ghg-inventories-2016>,
1150
1151 2016.
1152
- 1153 van der Walt, I. J., Neomagus, H. W. J. P., Nel, J. T., Bruinsma, O. S. L., and Crouse, P. L.: A
1154 kinetic expression for the pyrolytic decomposition of polytetrafluoroethylene, *J. Fluor. Chem.*,
1155 129, 4, 314-318, 10.1016/j.jfluchem.2008.01.003, 2008.
- 1156 Victor, D. G., and MacDonald, G. J.: A model for estimating future emissions of sulfur
1157 hexafluoride and perfluorocarbons, *Climatic Change*, 42, 4, 633-662, 1999.
- 1158 Vollmer, M. K., Mühle, J., Trudinger, C. M., Rigby, M., Montzka, S. A., Harth, C. M., Miller, B.
1159 R., Henne, S., Krummel, P. B., Hall, B. D., Young, D., Kim, J., Arduini, J., Wenger, A., Yao, B.,
1160 Reimann, S., O'Doherty, S., Maione, M., Etheridge, D. M., Li, S., Verdonik, D. P., Park, S.,
1161 Dutton, G., Steele, L. P., Lunder, C. R., Rhee, T. S., Hermansen, O., Schmidbauer, N., Wang, R.
1162 H. J., Hill, M., Salameh, P. K., Langenfelds, R. L., Zhou, L., Blunier, T., Schwander, J., Elkins, J.
1163 W., Butler, J. H., Simmonds, P. G., Weiss, R. F., Prinn, R. G., and Fraser, P. J. C. J. D.:
1164 Atmospheric histories and global emissions of halons H-1211 (CBrClF₂), H-1301 (CBrF₃), and
1165 H-2402 (CBrF₂CBrF₂), *J. Geophys. Res.*, 121, 7, 3663-3686, 10.1002/2015jd024488, 2016.
- 1166 Vollmer, M. K., Bernard, F., Mitrevski, B., Steele, L. P., Trudinger, C. M., Reimann, S.,
1167 Langenfelds, R. L., Krummel, P. B., Fraser, P. J., Etheridge, D. M., Curran, M. A. J., and
1168 Burkholder, J. B.: Abundances, emissions, and loss processes of the long-lived and potent
1169 greenhouse gas octafluorooxolane (octafluorotetrahydrofuran, c-C₄F₈O) in the atmosphere,
1170 *Atmos. Chem. Phys. Discuss.*, accepted for final publication, 2018, 1-20, 10.5194/acp-2018-852,
1171 2018a.
- 1172 Vollmer, M. K., Young, D., Trudinger, C. M., Mühle, J., Henne, S., Rigby, M., Park, S., Li, S.,
1173 Guillevic, M., Mitrevski, B., Harth, C. M., Miller, B. R., Reimann, S., Yao, B., Steele, L. P.,
1174 Wyss, S. A., Lunder, C. R., Arduini, J., McCulloch, A., Wu, S., Rhee, T. S., Wang, R. H. J.,
1175 Salameh, P. K., Hermansen, O., Hill, M., Langenfelds, R. L., Ivy, D., O'Doherty, S., Krummel, P.
1176 B., Maione, M., Etheridge, D. M., Zhou, L., Fraser, P. J., Prinn, R. G., Weiss, R. F., and
1177 Simmonds, P. G.: Atmospheric histories and emissions of chlorofluorocarbons CFC-13 (CClF₃),
1178 ΣCFC-114 (C₂Cl₂F₄), and CFC-115 (C₂ClF₅), *Atmos. Chem. Phys.*, 18, 2, 979-1002,
1179 10.5194/acp-18-979-2018, 2018b.
- 1180 Walters, D. N., Williams, K. D., Boutle, I. A., Bushell, A. C., Edwards, J. M., Field, P. R., Lock,
1181 A. P., Morcrette, C. J., Stratton, R. A., Wilkinson, J. M., Willett, M. R., Bellouin, N., Bodas-
1182 Salcedo, A., Brooks, M. E., Copsey, D., Earnshaw, P. D., Hardiman, S. C., Harris, C. M., Levine,
1183 R. C., MacLachlan, C., Manners, J. C., Martin, G. M., Milton, S. F., Palmer, M. D., Roberts, M.
1184 J., Rodríguez, J. M., Tennant, W. J., and Vidale, P. L.: The Met Office Unified Model Global
1185 Atmosphere 4.0 and JULES Global Land 4.0 configurations, *Geosci. Model Dev.*, 7, 1, 361-386,
1186 10.5194/gmd-7-361-2014, 2014.
- 1187 Zhihong, W., Seidel, S., Kokorin, A., and Rand, S.: Chapter 3.6, PFC, HFC, SF₆ emissions from
1188 semiconductor manufacturing, in: *IPCC Good Practice Guidance and Uncertainty Management in
1189 National Greenhouse Gas Inventories*, IGES, Hayama, Japan, 2001.
1190
1191



1192 **Tables**

1193 **Table 1.** Availability of $c\text{-C}_4\text{F}_8$ in situ, flask, firm, and aircraft air measurements, measurements sites, and instrumentation

Station/Site	Network	Lat.	Lon.	Medusa no.	Data availability*
Zeppelin (ZEP), Ny-Ålesund, Svalbard	AGAGE	78.9	11.9	19	09/2010–12/2017
NEEM08 firm, Greenland	–	77.5	-51.1	9	Extracted 07/2008
Summit13 firm, Greenland	–	72.7	-38.6	7	Extracted 05/2013
Mace Head (MHD), Ireland	AGAGE	53.3	-9.9	2	06/2010–12/2017
Tacolneston (TAC), United Kingdom	UK DECC/AGAGE	52.5	1.1	13	05/2013–12/2017
Jungfraujoch (JFJ), Switzerland	AGAGE	46.5	8.0	12	11/2008–12/2017
Monte Cimone (CMN), Italy	AGAGE/ICO-CV	44.2	10.7	ADS-GC/MS	05/2013–12/2017
Trinidad Head (THD), USA	AGAGE	41.0	-124.1	4	06/2010–12/2017
Shangdianzi (SDZ), China	AGAGE/CMA	40.7	117.1	17	05/2010–08/2012, 15/2015–04/2017, 09/2017–12/2017
Gosan (GSN), South Korea	AGAGE/KNU	33.3	126.2	10	06/2010–09/2016, 04/2017–09/2017, 12/2017–12/2017
La Jolla (SIO), USA	AGAGE	32.9	-117.3	1	11/2009–08/2013, 01/2014–12/2017
NH flasks	SIO & other	33–46	-72 – -124	7, 1, 9	10/1973–04/2016
Aircraft flask samples, India	FAAM/UoB	9–28	72–86	21	06/2016–07/2016
Ragged Point (RPB), Barbados	AGAGE	13.2	-59.4	5	06/2010–06/2014, 10/2014–12/2017
Cape Matatula (SMO), American Samoa	NOAA/AGAGE	-14.2	-170.6	6	08/2010–12/2017
Aspendale (ASA), Australia	AGAGE	-38.0	145.1	9	04–10/2010, 05–07/2011, 05/2015–12/2017
Cape Grim (CGO), Australia	AGAGE	-40.7	144.7	3	09/2010–12/2017
CGAA flasks, Australia	CSIRO/BoM	-40.7	144.7	9, 7	04/1978–12/2010
DSSW20K firm, Antarctica ⁺	–	-66.7	112.8	7	Extracted 12/1997
SPO01 firm, Antarctica	–	-90.0	-119	9	Extracted 01/2001

1194 *Shorter interruptions are excluded.

1195 AGAGE: Advanced Global Atmospheric Gases Experiment (Prinn et al., 2018).



1196 NEEM08: Firn air samples collected in 2008 at the Northern Greenland Eemian Ice Drilling Project, Greenland were collected by the University of Copenhagen,
1197 Denmark, the NEEM consortium, and the Commonwealth Scientific and Industrial Research Organisation (CSIRO) (Buizert et al., 2012).
1198 Summit13: Firn samples collected in 2013 near Summit station, Greenland by the University of Rochester and Oregon State University.
1199 UK DECC: The Tacolneston (TAC) site is part of the UK Deriving Emissions linked to Climate Change network (Stanley et al., 2018).
1200 DSSW20K: Firn samples collected in December 1997 at Dome Summit South West 20 km, Law Dome by CSIRO, the Australian Antarctic Division (AAD), and the
1201 Australian Nuclear Science and Technology Organisation (ANSTO) (see Trudinger et al., 2016 and citations therein).
1202 SPO01: Firn samples collected in 2001 at South Pole, Antarctica, by Bowdoin College, the National Oceanic and Atmospheric Administration (NOAA), the
1203 University of Colorado and the National Science Foundation (NSF) (Aydin et al., 2004; Sowers et al., 2005).
1204 ICO-OV: Measurements at the Italian Climate Observatory “O. Vittori” Monte Cimone (CMN) were performed with a commercial Adsorption-Desorption System
1205 with gas chromatograph and mass spectrometer (ADS-GC/MS) (Maione et al., 2013).
1206 CMA: China Meteorological Administration.
1207 KNU: Kyungpook National University, South Korea.
1208 SIO & other: Most archived northern hemispheric (NH) samples were collected by the Scripps Institution of Oceanography, La Jolla and measured on Medusa 7.
1209 FAAM/UoB: Air samples over India and the Indian Ocean were taken aboard the UK’s FAAM (Facility for Airborne Atmospheric Measurements) BAe-146 research
1210 aircraft and analyzed on Medusa 21 at University of Bristol (UoB) (Say et al., 2019).
1211 CGAA: Cape Grim Air Archive samples were collected by the CSIRO Oceans and Atmosphere and the Bureau of Meteorology (BoM), Australia predominantly
1212 measured on the Aspendale Medusa 9 at CSIRO (Langenfelds et al., 2014).
1213
1214
1215
1216
1217
1218
1219
1220
1221
1222



Table 2. Regional $c\text{-C}_4\text{F}_8$ emissions derived for eastern Asia from Gosan measurements (NAME-HB inversion) and comparison to global emissions (Gg yr^{-1} ; kt yr^{-1})

	Eastern China [#]	Western Japan [#]	South Korea	North Korea	Taiwan [#]	Σ eastern Asia	Global [†]	Global - Σ eastern Asia
2010	0.30 ± 0.07	0.02 ± 0.01	0.019 ± 0.008	0.008 ± 0.004	0.008 ± 0.005	0.36 ± 0.07	1.40 ± 0.11	1.04 ± 0.13
2011	0.35 ± 0.07	0.02 ± 0.01	0.016 ± 0.007	0.006 ± 0.003	0.007 ± 0.005	0.41 ± 0.07	1.52 ± 0.10	1.12 ± 0.12
2012	0.41 ± 0.06	0.02 ± 0.01	0.009 ± 0.005	0.004 ± 0.002	0.010 ± 0.008	0.45 ± 0.06	1.61 ± 0.08	1.16 ± 0.10
2013	0.46 ± 0.09	0.02 ± 0.01	0.017 ± 0.007	0.007 ± 0.004	0.008 ± 0.005	0.51 ± 0.09	1.67 ± 0.09	1.15 ± 0.13
2014	0.54 ± 0.06	0.03 ± 0.01	0.039 ± 0.009	0.009 ± 0.004	0.009 ± 0.006	0.62 ± 0.06	1.76 ± 0.09	1.14 ± 0.11
2015	0.59 ± 0.09	0.02 ± 0.01	0.041 ± 0.010	0.011 ± 0.005	0.011 ± 0.009	0.68 ± 0.09	1.88 ± 0.10	1.21 ± 0.13
2016	0.67 ± 0.12	0.02 ± 0.01	0.022 ± 0.010	0.009 ± 0.005	0.009 ± 0.006	0.73 ± 0.12	2.06 ± 0.10	1.33 ± 0.16
2017	0.68 ± 0.13	0.02 ± 0.01	0.014 ± 0.011	0.006 ± 0.005	0.010 ± 0.009	0.73 ± 0.13	2.20 ± 0.11	1.47 ± 0.17
a priori*	China 0.42 ± 0.05	Japan 0.09 ± 0.01	South Korea 0.032 ± 0.002	North Korea 0.010 ± 0.001	Taiwan 0.009 ± 0.001	Sum 0.56 ± 0.05		
a priori*	Eastern China 0.185	Western Japan 0.0294						

[†]Global emissions are the average of the emissions determined by the CSIRO and the Bristol inversion in this work.

[#]Eastern China contains the provinces Anhui, Beijing, Hebei, Henan, Jiangsu, Liaoning, Shandong, Shanghai, Shanxi, Tianjin and Zhejiang. Western Japan contains the prefectures Chugoku, Kansai, Shikoku and Okawa and Kyushu. Due to the lower sensitivities of the inversion in western China, eastern Japan, and parts of Taiwan, where potential source industries are located, we cannot exclude further emissions in these regions and therefore total emissions are probably larger.

*Saito et al. (2010) emission estimates based on atmospheric measurements from November 2007 to September 2009 were used as a priori information and were spread for each country uniformly over the area of each country. The resulting a priori estimates for eastern China and western Japan are additionally listed for comparison with the inversion results for these regions.

Gosan measurements started in June 2010 with most complete coverages from 2011 to 2015.

1223

1224

1225

1226

1227

1228

1229

1230

1231

1232

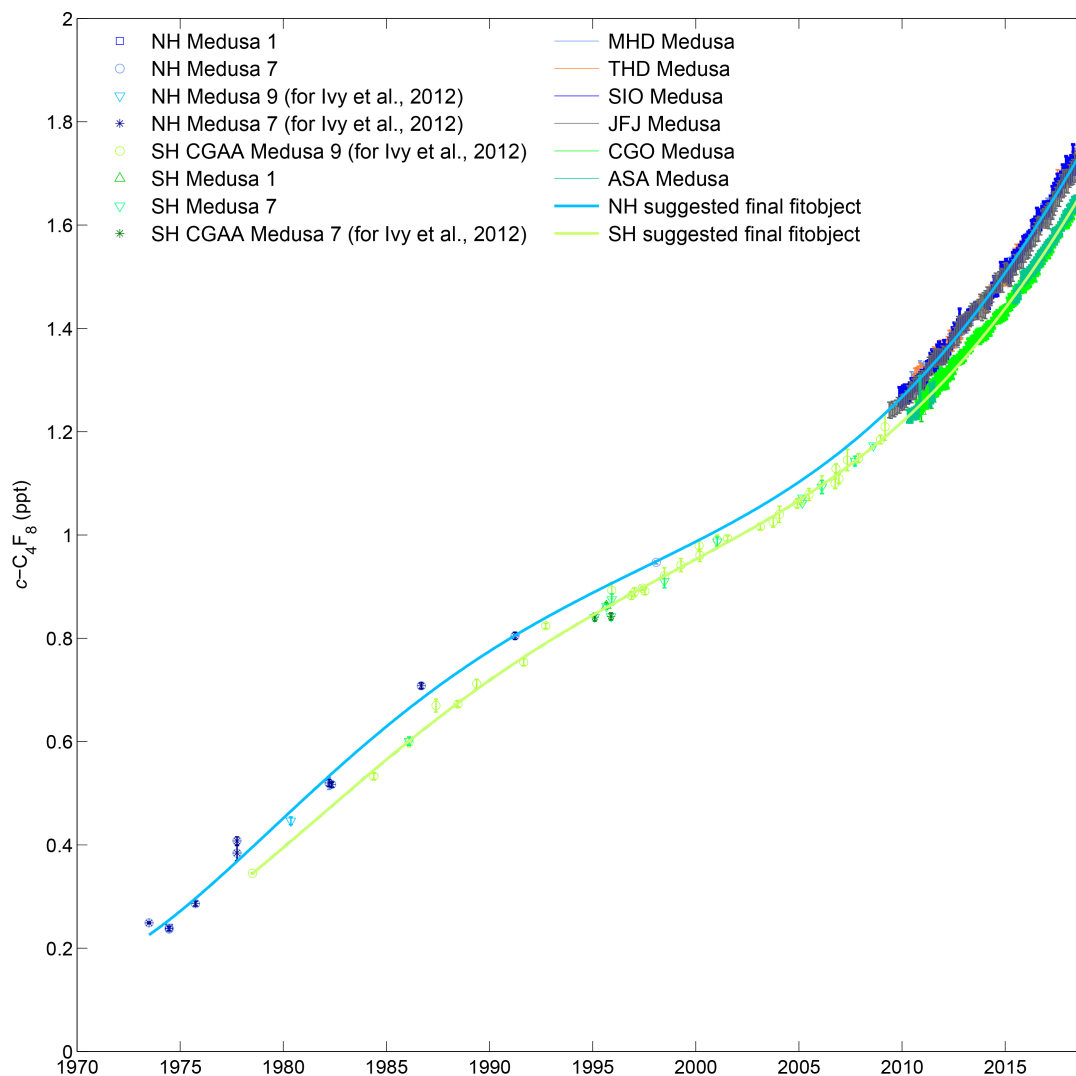
1233

1234

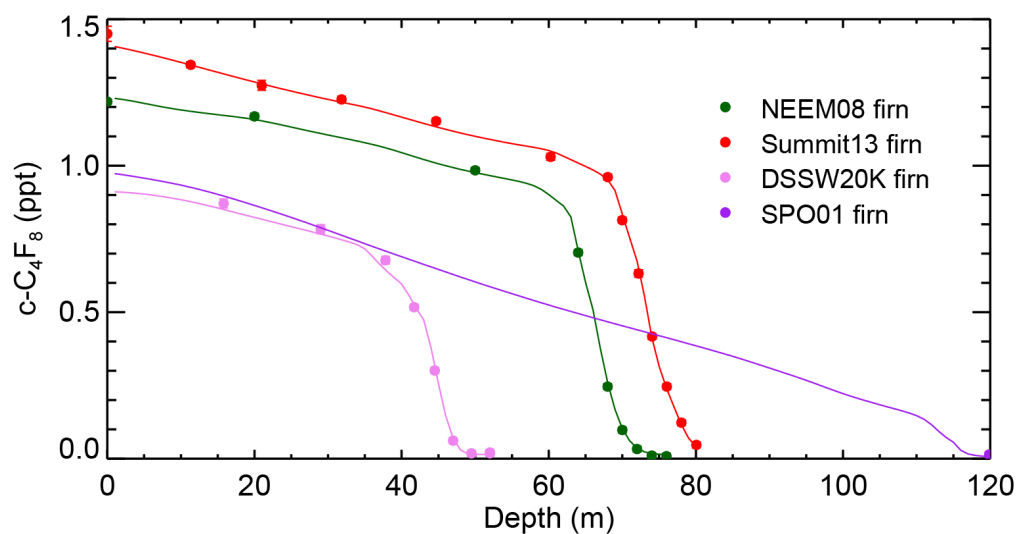
1235



1236 **Figures**



1237
1238 **Figure 1.** $c\text{-C}_4\text{F}_8$ mole fractions reconstructed from the late 1970s to 2018 from archived air samples and in situ
1239 measurements in both hemispheres. Cape Grim Air Archive (CGAA) and archived NH air samples are shown with
1240 symbols in shades of green and blue, respectively, reflecting different data subsets. For recent years, in situ
1241 measurements are shown as pollution removed monthly means for extra-tropical stations in the NH (MHD in light
1242 blue, THD in orange, SIO in darker blue, JFJ in grey) and in the SH (CGO in lighter green, ASA in pale green).
1243 Shown are the final data after an iterative filtering process described in the main text. The final suggested fits are
1244 shown as bold light green (SH) and bold light blue (NH) polynomial fits. Results for the tropical stations, RPB and
1245 SMO, the Asian stations, GSN and SDZ, and the Arctic station, ZEP, are omitted here for clarity.

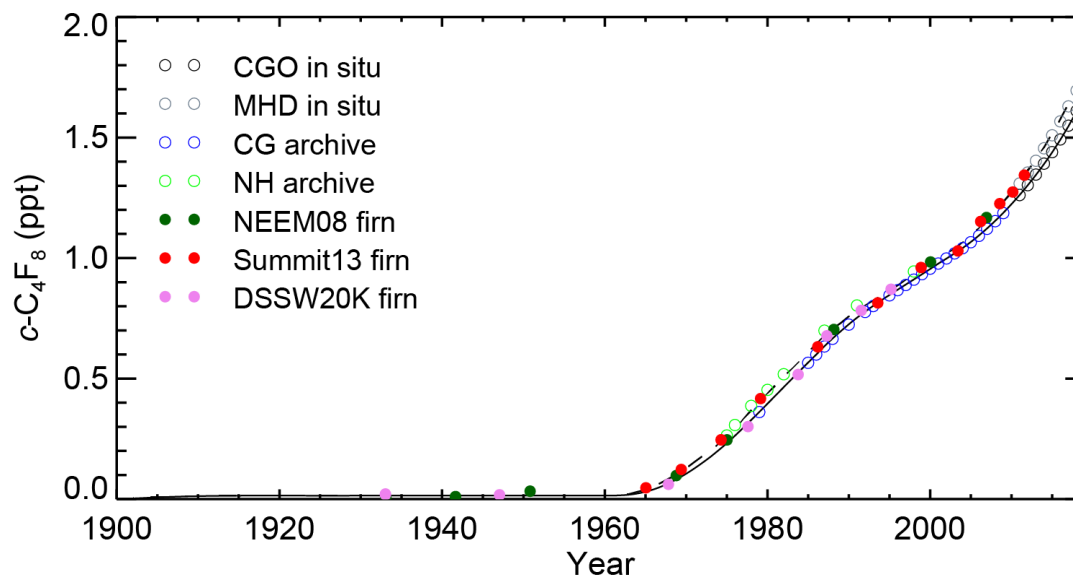


1246

1247 **Figure 2.** Depth profile of $c\text{-C}_4\text{F}_8$ measured dry-air molar mole fractions (parts per trillion, ppt) in air extracted from
1248 polar firn at NEEM08 (Northern Greenland, dark green) and Summit13 (Greenland, red) in the NH and DSSW20K
1249 (Eastern Antarctica, pink) and SPO01 (South Pole, purple) in the SH, together with the simulated depth profiles for
1250 each site (dark green, red, pink, and purple lines) that correspond to the emissions inferred by the CSIRO inversion.
1251 The modelled depth profiles for each site (solid lines) are based on the inversion of measurements from all firn sites,
1252 archive, and in situ data. Measurement precisions (1σ) are shown as error bars and are generally smaller than the
1253 plotting symbol.

1254

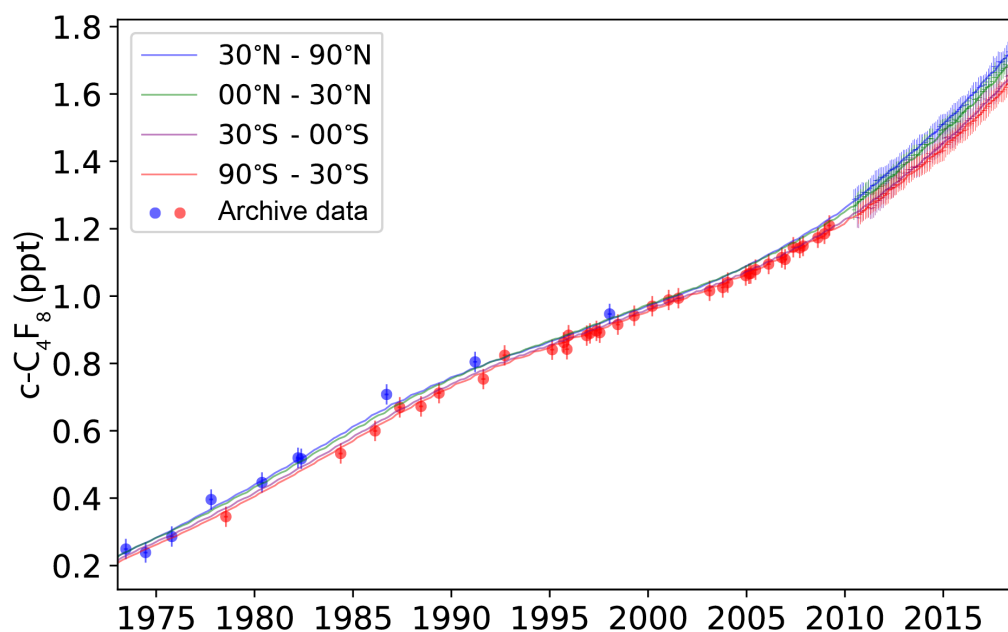
1255



1256

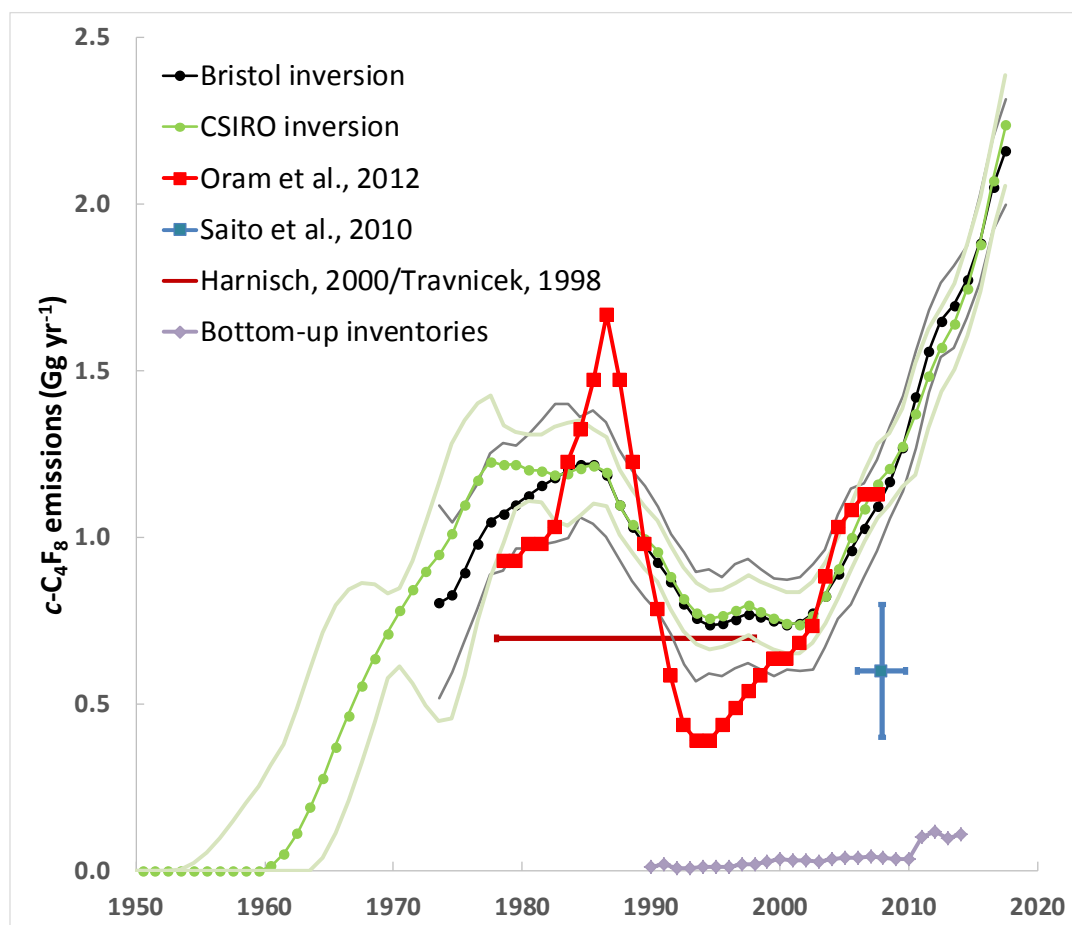


1257 **Figure 3.** Historic atmospheric $c\text{-C}_4\text{F}_8$ mole fractions reconstructed for the extra-tropical Northern and Southern
1258 Hemispheres from air extracted from polar firn (full circles, NEEM08 in dark green, Summit13 in red, DSSW20K in
1259 pink, against mean or effective ages; SPO01 with mean age of ~ 1890 is not shown), annual values from spline fits to
1260 Cape Grim Air Archive (CG archive, open blue circles) and in situ measurements at Cape Grim (CGO, open black
1261 circles), archived air samples (NH archive, open green circles) and in situ measurements at Mace Head (MHD, open
1262 grey circles). Also shown are reconstructed abundances based on optimized emissions determined by the CSIRO
1263 inversion for the extra-tropical SH (black line) and NH (dashed black line).
1264



1265 **Figure 4.** Historic $c\text{-C}_4\text{F}_8$ mole fractions from archive samples in both hemispheres (filled circles) and pollution free
1266 monthly mean in situ data from AGAGE background sites (MHD and THD in blue, RPB in green, SMO in purple
1267 and CGO in green, vertical bars, bar size represents variability of monthly means) are shown together with the
1268 Bristol inversion results for the four latitudinal bands represented by these background sites (30°N – 90°N , 0°N – 30°
1269 N , 0°S – 30°S and 30°S – 90°S , solid lines of same color).
1270

1271
1272
1273
1274
1275
1276
1277
1278



1279

1280 **Figure 5.** Global $c\text{-C}_4\text{F}_8$ emissions reconstructed by the CSIRO inversion (green dots and line, light green 2σ
1281 uncertainty bands) from 1950 and by the Bristol inversion (black dots and line, grey 1σ uncertainty bands) from the
1282 early 1970s to present. In situ and archive data are used in both inversions, while firm air data are only used in the
1283 CSIRO inversion. Emission estimates by Oram et al., 2012 (red), Saito et al., 2010 (blue), Harnisch, 2000/Travnicek,
1284 1998 (brown) and from available bottom-up inventory information (grey) are shown for comparison.

1285

1286

1287

1288

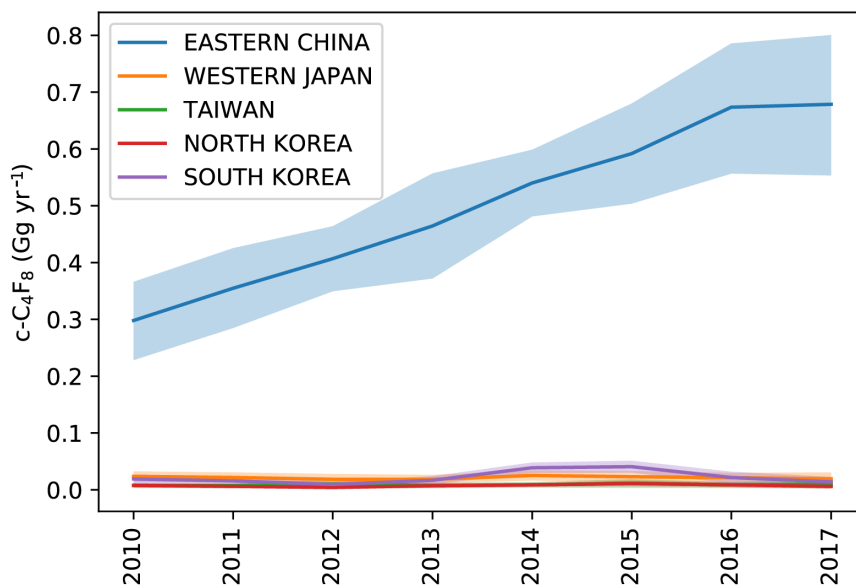
1289

1290

1291

1292

1293



1294

1295

1296 **Figure 6.** *c*-C₄F₈ emission in eastern Asia as determined by the NAME-HB regional inversion of measurements at

1297 the Gosan station, Jeju Island, South Korea are dominated by emissions from eastern China (blue), followed by

1298 emissions from western Japan (orange). Emissions from South Korea (violet) are much smaller, but show a small

1299 maximum in 2014 and 2015. Emissions from Taiwan (green) and North Korea (red) also small. Shadings represent

1299 uncertainty bands of emissions.

1300

1301

1302

1303

1304

1305

1306

1307

1308

1309

1310

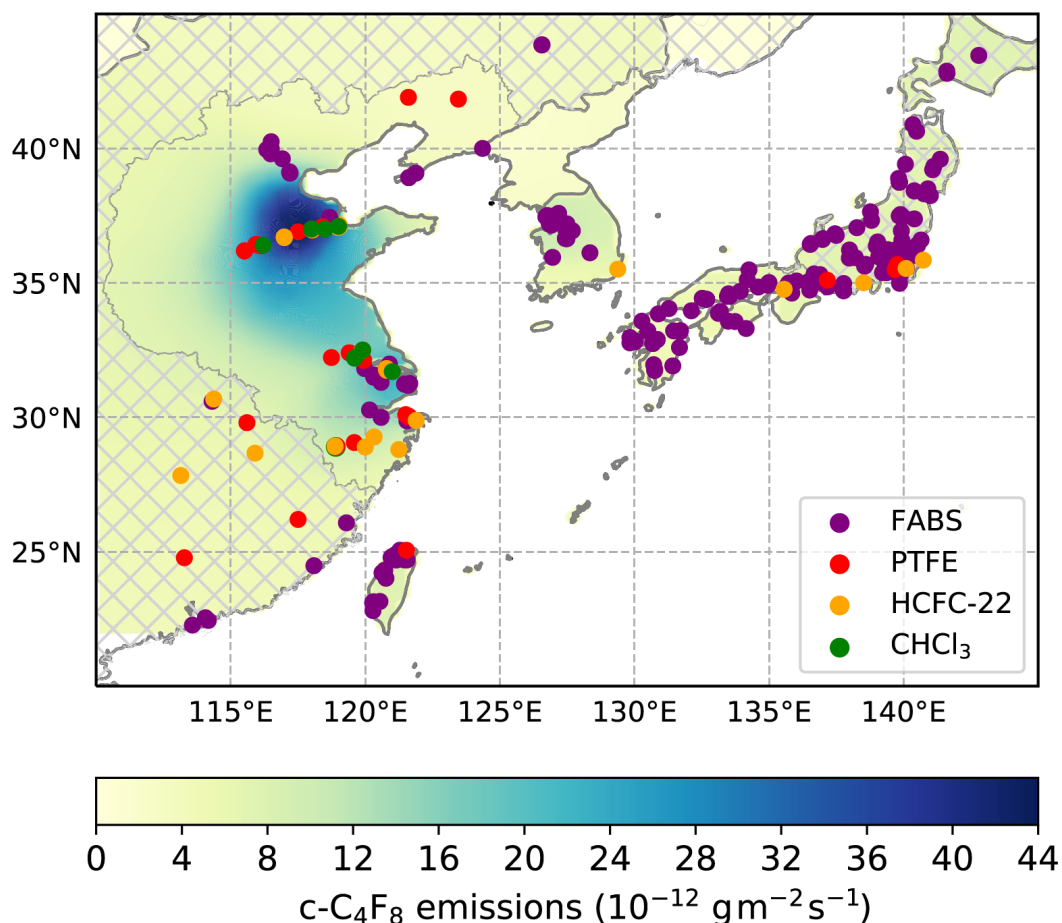
1311

1312

1313

1314

1315



1316

1317 **Figure 7.** Mean $c\text{-C}_4\text{F}_8$ emission strength (shades of green and blue, $10^{-12} \text{ g m}^{-2} \text{ s}^{-1}$) in eastern Asia from 2010 to

1318 2017 determined by the NAME-HB inversion from measurements at the Gosan station, Jeju Island, South Korea.

1319 The hatching indicates areas for which emissions are not reported due to relatively low sensitivities of the inversion.

1320 Emissions predominantly occur in the densely industrialized Shandong, Tianjin and parts of Henan and Hebei

1321 provinces south/southwest of Beijing as well as in Shanghai and neighboring provinces Jiangsu (to the north), Anhui

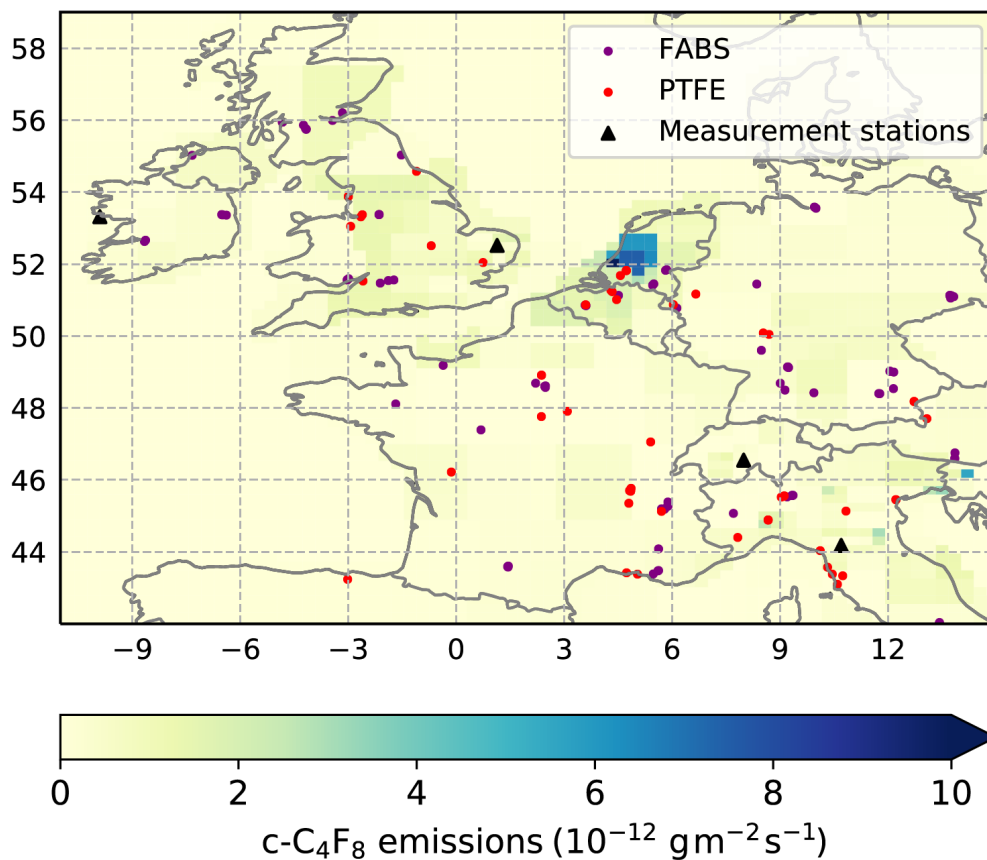
1322 (to the west) and Zhejiang (to the south) of the Yangtze River Delta region. Shown are industries with potential $c\text{-C}_4\text{F}_8$ 1323 emissions: Semiconductor fabrication plants (FABS, purple dots, [en.wikipedia.org/wiki/List_of_](https://en.wikipedia.org/wiki/List_of_semiconductor_fabrication_plants)1324 www.10stripe.com/featured/map/semiconductor-fabs.php and other sources) and1325 TFE/HFP/PTFE/FEP production facilities (PTFE, red dots, [www.qianzhan.com/analyst/detail/220/170629-](http://www.qianzhan.com/analyst/detail/220/170629-c33a2ca7.html)1326 [c33a2ca7.html](http://www.qianzhan.com/analyst/detail/220/170629-c33a2ca7.html) and other sources). HCFC-22 (orange dots) and chloroform (CHCl_3 , green dots) production facilities

1327 are shown as the TFE and HFP monomers needed to produce PTFE and FEP fluoropolymers are produced via

1328 pyrolysis of HCFC-22 and $c\text{-C}_4\text{F}_8$ is an intermediate/by-product in this process, while HCFC-22 is manufactured1329 from CHCl_3 .

1330

1331



1332

1333

1334 **Figure 8.** Mean $c\text{-C}_4\text{F}_8$ emission strength (shades of green and blue, $10^{-12} \text{ g m}^{-2} \text{ s}^{-1}$) in North Western Europe (42° N 1335 to 59° N and -11° E to 15° E) from 2013–2017 determined by the InTEM inversion from measurements at four sites

1336 (Mace Head, Ireland, Tacolneston, United Kingdom, Jungfraujoch, Switzerland, and Monte Cimone, Italy, black

1337 triangles). Also shown are potential industrial emitters of $c\text{-C}_4\text{F}_8$. Locations of potential TFE/HFP/PTFE/FEP

1338 production facilities (red dots) are based on company websites (3M, Chemours, Daikin, DuPont, Saint-Gobain, and

1339 Solvay) and are much less certain than the corresponding location information for eastern Asia. Also shown are

1340 semiconductor fabrication plants (purple dots, en.wikipedia.org/wiki/List_of_semiconductor_fabrication_plants,1341 www.10stripe.com/featured/map/semiconductor-fabs.php, and other sources).

1342

1343

1344

1345

1346

1347

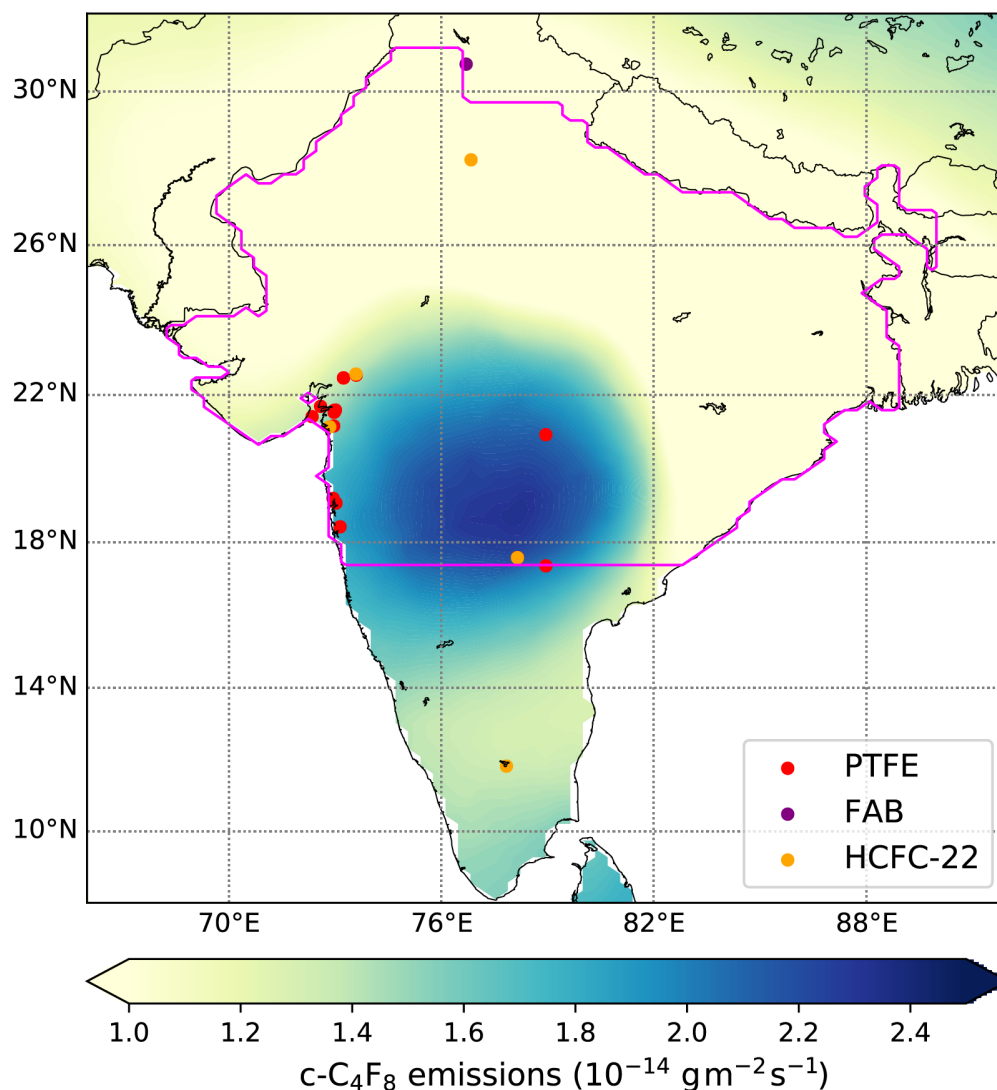
1348

1349

1350

1351

1352



1348

1349 **Figure 9.** Mean $c\text{-C}_4\text{F}_8$ emission strength (shades of green and blue, $10^{-14} \text{ g m}^{-2} \text{ s}^{-1}$) over the Indian subcontinent for
1350 June and July 2016 determined by the NAME-HB inversion based on air samples taken on-board UK's FAAM
1351 (Facility for Airborne Atmospheric Measurements) BAe-146 research aircraft. Also shown are the locations of one
1352 semiconductor fabrication plant (FAB, purple dot) and several potential PTFE/FEP production facilities (PTFE, red
1353 dots, Solvay/CYTEC, Hindustan Fluorocarbons, and Gujarat Fluorochemicals facilities) as potential $c\text{-C}_4\text{F}_8$ sources.
1354 HCFC-22 (orange dots) production facilities are also shown as the TFE and HFP monomers needed to produce PTFE
1355 and FEP fluoropolymers are produced via pyrolysis of HCFC-22 and $c\text{-C}_4\text{F}_8$ is an intermediate/by-product in this
1356 process. The outline of the Northern and Central India (NCI) model domain is shown as a pink line.

1357